Mémoire

Auteur : Pujol, Cécile
Promoteur(s) : Alvera Azcarate, Aida; 14934
Faculté : Faculté des Sciences
Diplôme : Master en océanographie, à finalité approfondie
Année académique : 2020-2021
URI/URL : http://hdl.handle.net/2268.2/12843

Université de Liège – University of Liège

Faculté des Sciences – Faculty of Sciences

Mémoire de fin d'études – Master's Thesis

Marine heatwaves offshore Central and South Chile: a global assessment and the case study of the year 2016

February 1st, 2021 - August 30th, 2021

Cécile Pujol

En vue de l'obtention du diplôme – Submitted in fulfilment of the requirements for

Master en Océanographie – Master's Degree in Oceanography

Promotrice – Promotor: Aida Alvera-Azcárate (*GeoHydrodynamics and Environment Research, Liège, Belgium)*
Co-promoteur – Co-promotor: Iván Pérez-Santos *(i~mar, Perto Montt, Chile)*

Année académique – Academic year: 2020-2021

Conformément aux règles imposées à la rédaction, ce mémoire ne doit pas dépasser 50 pages, rédigées en Times 12 ou équivalent.

In accordance with the writing directives, this Master's Thesis must not exceed 50 pages, written in Times 12 or equivalent.

Ce Mémoire a débuté le 1er février 2021 et a été rendu le 30 août 2021.

This Master's Thesis started on February 1st, 2021 and finished on August 30th, 2021.

Membres du jury – Jury members

Aida Alvera-Azcárate (promotor)

Iván Pérez-Santos (co-promotor)

Alexander Barth

Bruno Delille

Marilaure Grégoire

UNIVERSITY OF LIÈGE

Faculty of Sciences

Department of Astrophysics, Geography and Oceanography

Abstract

Master's Degree in Oceanography

Marine heatwaves offshore Central and South Chile: a global assessment and the case study of the year 2016

by Cécile PUJOL

Marine heatwaves (MHWs) are discrete warm-water anomalies events occurring in every ocean around the globe, in both coastal and open ocean, having major impacts on ecosystems, fisheries and aquaculture. Although processes leading to MHWs formation are becoming more and more studied since the beginning of the 2010s, the way they interact together to trigger MHWs remains not fully understood. Nevertheless, their link to human-induced global warming tends to be certain. The southern part of Chile (41°5'S - 56°S) is characterized by fjord ecosystems already experiencing global warming consequences, whether large-scale or local climate modifications. However, to the best of our knowledge, MHWs occurrence in Southern Chile has never been subject to studies, despite the fjord ecosystem's vulnerability to climate warming. Therefore, we assessed a global analysis of the MHWs that have occurred between 1982 and 2020 along Central and South coastal Chile, from 29°S to 55°S. We found that the last decade was record-breaking in terms of duration, intensity and occurrence of MHWs. In 2016, succession of MHWs during austral autumn, winter and spring lead to the formation of the longest (148 days, almost 5 months) and most extreme events (2.25°C above the climatology) ever recorded along Chile between 1982 and 2020. Those events were due to the advection of warm-waters anomalies coming from the open ocean and combination of persisting high pressure system with lower winds having led to reduced heat transfer from the ocean to the atmosphere. In addition, a global context of positive phases of El Niño Southern Oscillation and Southern Annular Mode contributed to the MHWs formation.

Key words: marine heatwave, Patagonia, Pacific Ocean, sea surface temperature anomaly, Southern Annular Mode, El Niño Southern Oscillation

UNIVERSITÉ DE LIÈGE

Faculté des Sciences

Département d'Astrophysique, de Géographie et d'Océanographie

Résumé

Master en Océanographie

Marine heatwaves offshore Central and South Chile: a global assessment and the case study of the year 2016

par Cécile PUJOL

Les vagues de chaleur marine, ou marine heatwaves (MHWs), sont des évènements discrets caractérisés par des eaux anormalement chaudes. Elles se produisent dans tous les océans, que ce soit en milieu côtier ou en pleine mer, et impactent fortement les écosystèmes marins, mais également les pêcheries et l'aquaculture. Bien que les processus menant à la formation de tels évènements soient de plus en plus étudiés depuis le début des années 2010, les interactions qu'ils ont entre eux pour conduire à la formation de MHWs restent encore relativement méconnues. Il est cependant de plus en plus certain que les MHWs sont liées au réchauffement climatique anthropique. Le sud du Chili (41°5'S – 46°S) est constitué d'un ensemble de fjords où les conséquences du réchauffement climatique se font déjà ressentir, que ce soient des modifications climatiques à l'échelle locale ou régionale. Cependant, d'après nos connaissances, il n'y a jamais eu d'étude portant sur les MHWs dans cette région du monde. Par conséquent, nous avons réalisé une étude globale des MHWs qui se sont produites entre 1982 et 2020 le long des côtes du Centre et du Sud du Chili, de 29°S à 55°S. Nous avons trouvé que la dernière décennie a été marquée par des MHWs particulièrement longues et fortes, et qu'elles se sont produites en plus grand nombre. En 2016, plusieurs MHWs se sont succédées de l'automne jusqu'au printemps australs, conduisant à la formation de la plus longue MHW (148 jours) et de la plus extrême (2.25°C au-dessus de la climatologie). Ces MHWs se sont produits suite au transport près des côtes d'eaux anormalement chaudes en provenance du Pacifique extratropical, associées à des hautes pressions stationnaires et une réduction des vents conduisant à une diminution des échanges de chaleur entre l'océan et l'atmosphère, en partie liés à des phases positives de El Niño Southern Oscillation et du Southern Annular Mode.

Mots clés : marine heatwave, Patagonie, Océan Pacifique, température de surface de l'océan, Southern Annular Mode, El Niño Southern Oscillation

Acknowledgments

I especially want to thank Aida for her endless help, her support and for the opportunities she gave me. More specifically, I want to thank her for having adapted the subject of the Master's Thesis with what I was interested in and to have always given good advice.
Above all, thank you for always being cheerful.

I want to thank Iván Pérez-Santos for having trusted me, for his support and above all for his endless knowledge of Patagonia.

Manal and Kene, without you I would not have such results so thank you very much.

Thanks to all the coffee-members for all your helpful advice and your precious presentations.

Special thanks to Jonathan, Séverine, Anne and my family for our discussions, your help and your support.

This work is dedicated to Flipie

TABLE OF CONTENT

TABLE OF ABBREVIATIONS

CHC	Cap Horn Current
ENSO	El Niiño Southern Oscillation
HAB	Harmful algal bloom
HCS	Humboldt Current System
MHW	Marine heatwave
PDO	Pacific Decadal Oscillation
Qb	Surface net termal radiation
Qc	Sensible heat flux
Qe	Surface latent heat flux
Qi	Total net heat flux
Qs	Surface net solar radiation
SAM	Southern Annular Mode
SPC	South Pacific Current
SPSA	South Pacific subtropical anticyclone
SST	Sea surface temperature

1 INTRODUCTION

1.1 Chile and Patagonia

1.1.1 Geographical zone

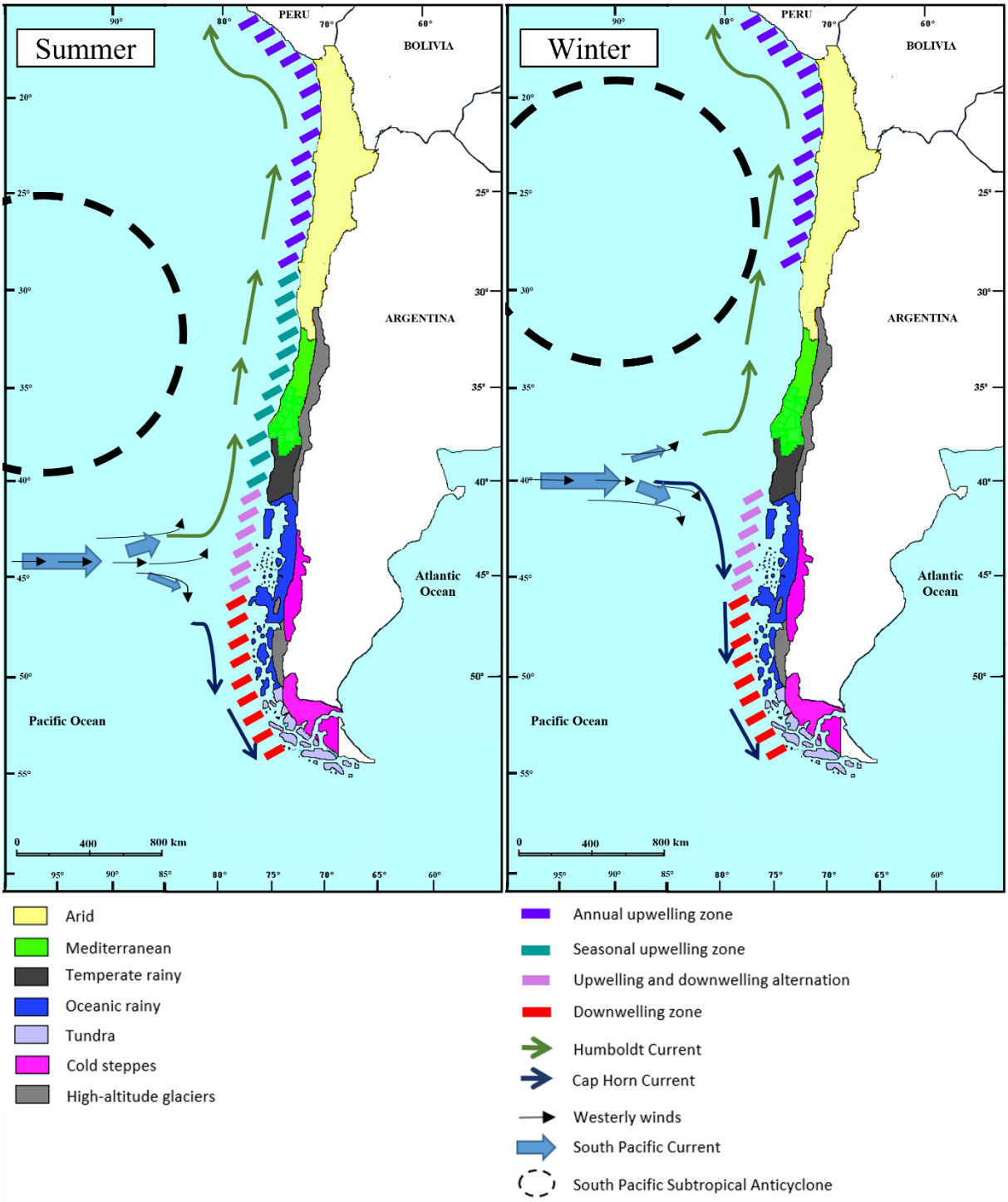

Figure 1: Schematic representation of the marine and atmospheric main processes off Chile and main climatic regions. Map modified from www.southernchileproperties.com

Chile, bordered to the West by the South Pacific Ocean and to the East by the Andean Cordillera, extends over more than 4 300 km from 17°S to 56°S (Figure 1). The Northern part of Chile extends from 18.4°S to 41.5°S and is characterized by a straight coast with cliffs, wetlands, dune fields, peninsulas and bays, whereas the southern part, named Patagonia, extends from 41.5°S to the southernmost point and is much more complex with a fragmented coast forming one of the largest fjords and channels region in the world *(Pantoja et al., 2011)*. The Andean Cordillera is especially important for climate modulation in Chile as it creates an altitudinal gradient and strongly interacts with atmospheric circulation *(McPhee et al., 2021)*. Indeed, with a maximum altitude in Chile of 6893 m at Ojos del Salado (27,1°S), the Cordillera is responsible for climate isolation of Chile from the South American continent *(e.g. Aceituno et al., 2021)*, by regulating precipitations and causing extreme drought climate in the Northern part of Chile (precipitation < 10 mm/year; *Aceituno et al., 2021)*, Mediterranean climate in central Chile, a hyper-humid region caused by the orographic effect of the Andes with precipitations superior 3 000 mm/year in Northern Patagonia and up to 7 000 mm/year in Central Patagonia (Figure 1; *Viale & Garreaud, 2015; Aceituno et al., 2021)*, and temperate wet and glacial environments in central and South Patagonia *(McPhee et al., 2021)*. In addition, the Cordillera has a major role in Chilean hydrology as most of the rivers originate from the glaciers melting, with an increasing number of rivers as we go South *(McPhee et al., 2021)*.

1.1.2 Atmospheric and oceanic circulation off Chile

1.1.2.1 Main atmospheric and oceanic systems

Climate and oceanic circulation off Chile are forced by large scale atmospheric systems (Figure 1). The two main atmospheric systems are the Westerly Winds belt at midlatitudes and the basin-scale South Pacific Subtropical Anticyclone (SPSA) extending over the Southeast Pacific, also named South Pacific High.

The Westerly Wind belt are jet-like eastward winds blowing at mid-latitude over the South Pacific Ocean. They are the main forcing of the South Pacific Current (SPC), an eastward current following the Westerly Winds at mid-latitudes between New-Zealand and Chile and forming the south branch of the South Pacific Gyre *(Stramma et al., 1995; Strub et al., 2019)*. Because of the orographic effect of the Andean Cordillera, Westerly Winds produce high precipitation over Chile *(Viale & Garreaud, 2015)*. When reaching the Chilean Coast, between 40 and 50°S, the SPC splits in two branches: a poleward current named the Cap Horn Current (CHC) and an equatorward current feeding the Humboldt Current System (HCS; *Strub et al., 2019)*. The HCS is one of the 4 major eastern boundary current systems, characterised by

intense, cold and nutritious-rich equatorward current, bounded to the North by equatorial currents *(Thiel et al., 2007)*. It is mostly known because it induces the formation of one of the most productive wind-driven upwelling systems in the world along Peruvian and northern Chilean coasts *(Chavez et al., 2008)*. Conversely, the CHC is a poleward buoyancy-driven coastal current, downwelling favourable from ~45°S to South Patagonia and strongest during winter with inputs from local rivers runoff *(Thiel et al., 2007)*.

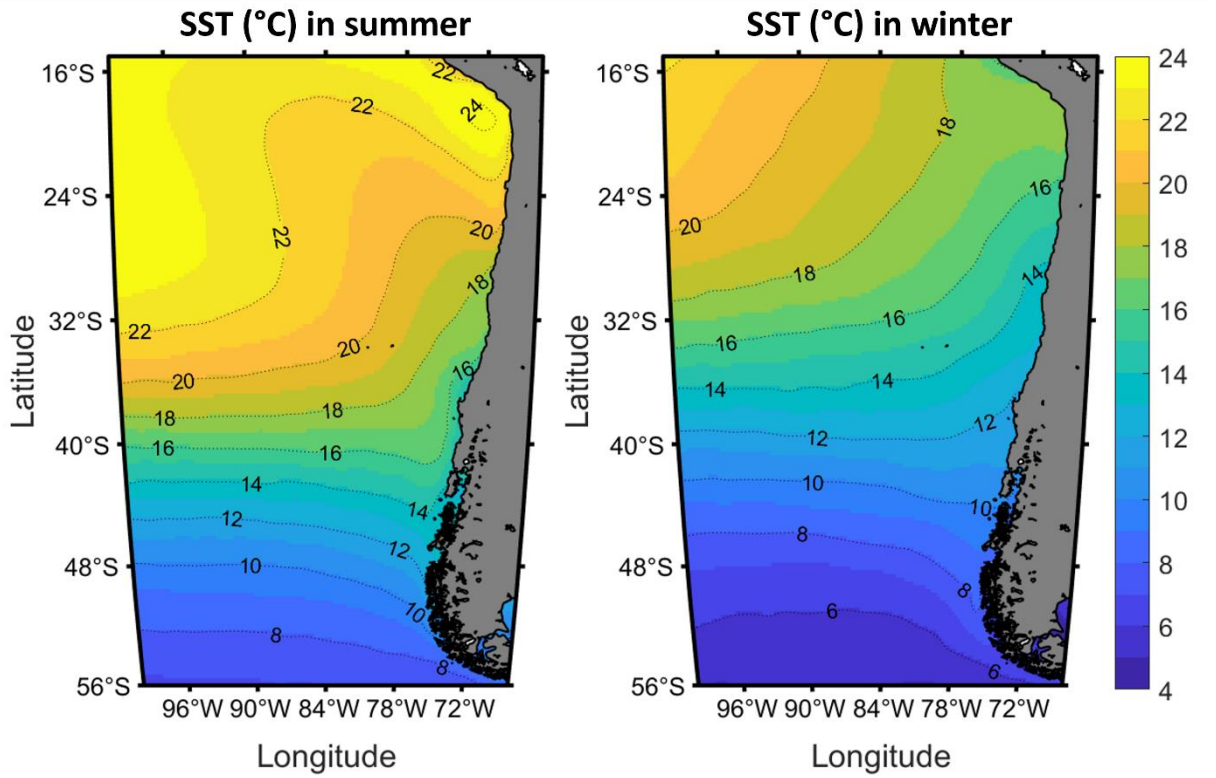

Figure 2: Mean sea surface temperature (SST; °C) in Southeast Pacific during summer (left) and winter (right). Seasonal averaged SST has been calculated over 1982-2020. In summer, SST is warmer along the coast and the North-South temperature gradient is stronger than in winter.

The SPSA is a permanent anticyclone with North-South migrations controlling the temperature distribution (both oceanic and continental) over Southeast Pacific Ocean and particularly over Chile with relatively warm conditions during summer and cold during winter (Figure 2). The SPSA is the main forcing of the subtropical oceanic gyre, which is bounded on the East part by the HCS *(Ancapichún & Garcés-Vargas, 2015)*. As the SPSA is constrained by the Andes on its East side, intense equatorward jet-like winds blow along the Chilean coasts *(Montecinos & Gomez, 2010)*. In addition, the SPSA is responsible for a strong seasonality of rainfall in Central Chile (30-40°S), more intense during austral winter *(Aceituno et al., 2021)*.

1.1.2.2 Seasonal variability

Forced by solar radiation, Westerly winds and SPSA are constrained to seasonal

migrations, thus inducing seasonal variability to currents and upwellings (Figure 1). During austral summer and spring, the SPSA is at its southernmost point, centred on ~100°W and 35°S and at its northernmost point during austral fall and winter, centred on ~90°W and 27°S *(Rahn & Garreaud, 2014)*. Consequently, due to the SPSA convergence to the coast in winter, wind-driven upwellings in the northern part of Chile are stronger in winter than in summer *(Ancapichún & Garcés-Vargas, 2015)*. Westerly winds also have a seasonal cycle, coordinated with the SPSA seasonal migration, going southward (~45°S) in summer and northward (35°S-40°S) in winter *(Thiel et al., 2007)*. Consequently, in South-Central Chile and Northern Patagonia, winds alternate with equatorward direction during summer and poleward direction during winter (Figure 1).

The North-South migration of the two main atmospheric systems is largely influencing the oceanic circulation. Indeed, at mid-latitudes, the SPC migrates in combination with westerly winds, reaching southern coast in summer and northern coast in winter (e.g. *Strub et al., 2019)*. Thus, the wind-induced currents are also alternating from North to South direction along central Chile with respectively equatorward currents in summer and poleward currents in winter along central coasts of Chile *(e.g. Thiel et al., 2007; Strub et al., 2019)*. It is admitted that between 18°S and 28°S, seasonal variability for both winds and currents is low *(Pizarro et al., 1994)*. Although currents seasonality exists south of 30°S, different studies agree to say that North of 37°S wind and currents are nearly always equatorward (upwelling favourable; *e.g. Sobarzo et al., 2007*). Further South, although it is still discussed, south of 46°S currents would be nearly always poleward (downwelling favourable; *Strub et al., 2019)*. Between 37°S and 46°S, there is a zone where the currents alternate from equatorward direction in summer to poleward direction in winter, which has been named "transition zone" by Strub et al. (2019). Therefore, in the transition zone, there are upwellings favourable conditions in summer associated with cold SST and high chlorophyll-*a* concentration, and downwelling favourable conditions during winter with opposite features (Figure 1; *Rahn & Garreaud, 2014; Strub et al., 2019).*

On top of that, wind, currents and upwellings also have an interannual and decadal variability forced by, among others, El Niño Southern Oscillation (ENSO), Pacific Decadal Oscillation (PDO) and Southern Annular Mode (SAM; see section 1.1.2.3).

1.1.2.3 Remote forcings

El Niño Southern Oscillation

El Niño Southern Oscillation (ENSO) is an irregular cyclic atmospheric phenomenon,

occurring every 2 to 7 years, influencing primarily the Equatorial Pacific Ocean *(NOAA Climate, 2014; Chen, Thual, & Hu, 2019)*. ENSO is regulated by the Walker circulation, induced by a pressure gradient between Eastern and Western Pacific Ocean: a high-pressure system over the eastern part and a low-pressure system over Indonesia, resulting in strong westward Tradewinds *(Chen, Thual, & Stuecker, 2019)*. This Walker circulation causes an upwelling system along Central America coasts associated with a shallow thermocline and conversely warm waters accumulation over South-eastern Asia and Northern Oceania with a deep thermocline. ENSO is composed of 2 distinct phases: a warm phase called El Niño and a cold phase called La Niña. An El Niño (La Niña) phase corresponds to a weaker (stronger) than usual Walker circulation: Tradewinds are weaker (stronger), the thermocline is deeper (shallower) and its slope is reduced (increased), the upwellings are reduced (enhanced) and the pressure gradient between Western and Eastern Pacific is reduced (enhanced; Figure 3; *Santoso et al., 2017)*.

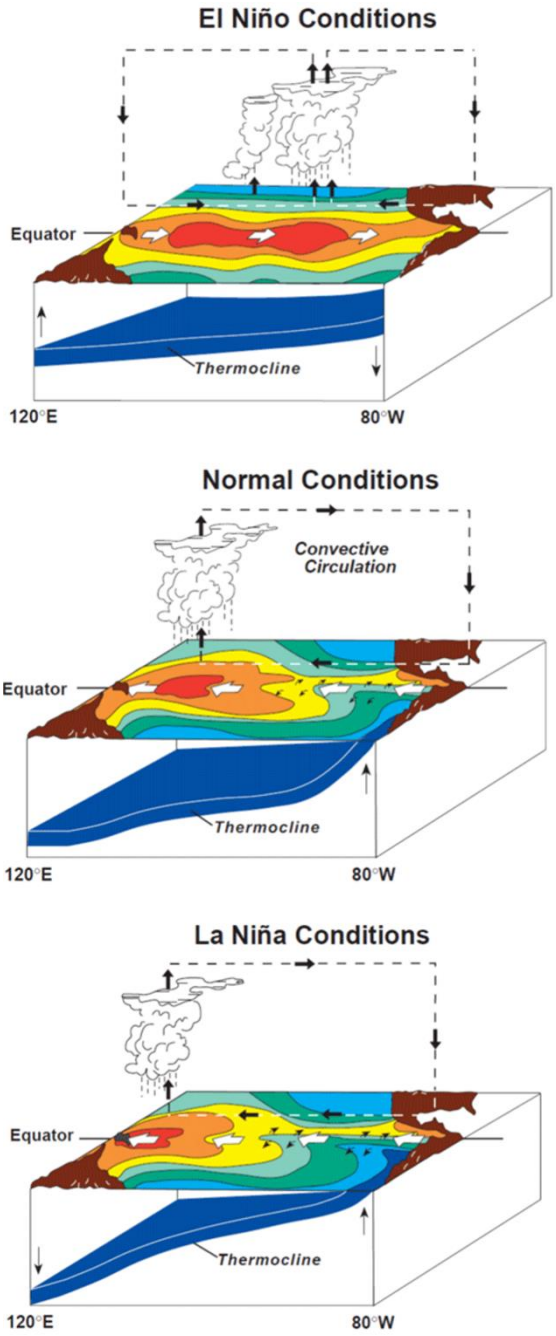

Figure 3: Schematic representation of the Walker circulation with (top) El Niño condition associated with deep thermocline along Americas and eastward propagation of warm surface waters, (centre) neutral condition, (bottom) La Niña conditions associated with shallower thermocline along Americas. Warmer colours represent warmer waters. Chen, Thual, & Hu, 2019

In Chile, ENSO can modify oceanic conditions, leading to a deeper thermocline during El Niño (warm) periods, and weaken the SPSA (reverse conditions during La Niña; *Ancapichún & Garcés-Vargas, 2015)*, having consequences on upwellings regimes by modulating their onset and end *(Montecinos & Gomez, 2010)*. In addition, when an El Niño (La Niña) event occurs, Westerly Winds are reduced *(Rind et al., 2001)* and summers in Chile are wetter (dryer) than usual *(Montecinos & Aceituno, 2003)*.

Pacific Decadal Oscillation

The Pacific Decadal Oscillation (PDO) is an ocean fluctuation, often described as an ENSO-like pattern variability *(Mantua et al., 1997; Mantua & Hare, 2002; Newman et al., 2016)* but over longer timescale (20 to 30 years). The warm (cold) phase of PDO provokes anomalously warm (cold) SST along the tropical coasts of both North and South America *(e.g. Mantua et al., 1997)*. PDO can attenuate ENSO influences when their phases are opposites and strengthen ENSO effects when phases are combined *(Yáñez et al., 2017)*. PDO consequences over Central Chile are ENSO-like, with drought (wet) conditions during cold (warm) phases *(Garreaud et al., 2009; Ancapichún & Garcés-Vargas, 2015)*.

Southern Annular Mode

The Southern annular mode (SAM), also called Antarctic Oscillation, is the principal mode of variability of the extratropical circulation in the Southern hemisphere centred on Antarctica and influencing high and mid-latitude climate *(Estay & Lima, 2010; Lee et al., 2019)*. It appears throughout the year in the troposphere, though it can also extend to the stratosphere in spring when its activity is stronger, and is characterized by large scale alternation of atmospheric mass between high latitude and mid-latitude surface pressure *(Gong & Wang, 1999; Thompson & Wallace, 2000; Reboita et al., 2009)*. Thompson & Wallace (2000) define the SAM as a geopotential height perturbation of opposite signs in Antarctica and at mid-latitudes (Figure 4).

SAM influences the Southern hemisphere atmospheric circulation by inducing a North-South oscillation of mid-latitude westerly winds thus impacting climate *(Thompson & Wallace,*

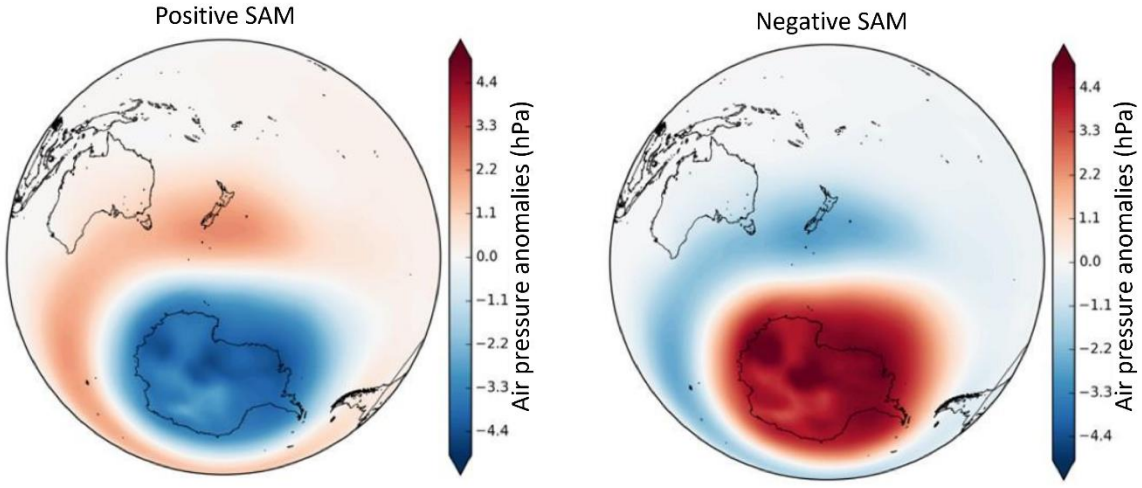

Figure 4: Schematic representation of positive (left) and negative (right) phases of SAM, centred on New-Zealand. Shaded-red areas indicate higher than average pressure anomalies whereas shaded-blue areas indicate lower than average pressure anomalies (hPa). National Institute of Water and Atmospheric Research

2000). Indeed, there is a strong negative correlation between 40°S and 60-70°S zonal mean sea level pressure: when atmospheric pressure is high at 40°S, atmospheric pressure is lower at 60-70°S and conversely *(Gong & Wang, 1999)*. When the pressure is lower (higher) in Antarctica and higher (lower) at mid-latitude, it is a positive (negative) phase of SAM. When positive (negative) SAM occurs, Westerly Winds position is moving poleward (equatorward) and are weaker (stronger) near 40°S, associated to a precipitation decrease and highest temperatures over Western Patagonia *(Gong et al., 2010; Garreaud, 2018; Lee et al., 2019)*.

Co-occurrence of ENSO and SAM

It has been shown that ENSO and SAM are not independent events *(L'Heureux & Thompson, 2006; Ding et al., 2012; Wang & Cai, 2013)*. Indeed, ENSO may force SAM occurrence via Rossby wave trains forced by warm SST anomalies in the Tropical Pacific Ocean during ENSO phases. In fact, La Niña (El Niño) conditions favour strong (weak) anticyclonic wave breaking on the equatorward side of the westerly winds jet *(Gong et al., 2010)*. These wave breakings are driving positive (negative) SAM phases *(Gong et al., 2010)*. However, when same-sign ENSO and SAM phases occur together, their effects add up, especially over Northern and Central Patagonia with for instance weaker winds, reduced precipitation or higher SST during positive phases *(Garreaud, 2018)*.

1.1.3 Chile facing climate change

According to the general index of climate risk *(see Eckstein et al., 2018)* established for 2019, Chile would be the 16th country more at risk from global warming effects. Indeed, with large arid and semi-arid regions prone to extend with global warming, precipitations mostly dependent on the Westerly Winds and glaciers melting, Chile is particularly vulnerable to climate change *(Yáñez et al., 2017)*. However, in Patagonia, climate change effects are not fully studied, but the general statement is that the region would experience drier conditions and a weak warming *(Garreaud et al., 2013; Boisier et al., 2016)*. Indeed, since 2010, long drought periods are occurring more frequently than in the past *(Garreaud, 2018; Winckler-Grez et al., 2020*). Those climate changes are mainly caused by a decrease of the Westerly Winds' intensity since the 1990s, attributed to SAM positive trends and anthropogenic climate change *(Gillett & Thompson, 2003; Garreaud et al., 2013)*. As Westerly Winds are the main precipitation driver in Patagonia, their weakening has reduced precipitation rate, especially during summer *(León-Muñoz et al., 2018)*. In addition, a poleward shift and a strengthening of the SPSA was observed since the 1990s *(Ancapichún & Garcés-Vargas, 2015; Aguirre et al., 2018; Winckler-Grez et al., 2020; Zou & Xi, 2021)*. The southward migration of the SPSA, transporting warm dry air,

would intensify the warm and drought episodes *(Flores-Aqueveque et al., 2020)*. As a consequence, reduction of precipitations would reduce rivers discharge, strongly impacting human freshwater access but also coastal ecosystems by modifying nutrient supply, turbidity and salinity *(e.g. Soto et al., 2019; Winckler-Grez et al., 2020)*. In addition, coastal ecosystems, particularly fjords ones, would also be affected by the glaciers melting, already melting for some of them *(e.g. Porter & Santana, 2014)*, by modifying river discharge.

Not only global warming would affect fjords ecosystems but also Chilean aquaculture. Indeed, because of the stable cold temperate-oceanic climate and the high number of rivers, Chile has developed a large part of its economy in fresh, brackish and sea water aquaculture (whose 90% is farmed in Patagonia), being the 5th world biggest producer of aquaculture products and the second biggest salmon producer and exporter after Norway *(Iriarte, 2018; FAO, 2019)*. Global warming may lead to unfavourable conditions for Patagonian aquaculture farming, in addition to the already existing hypoxic conditions *(e.g. Schneider et al., 2014; Silva & Vargas, 2014)*, by increasing both atmospheric and sea temperature, modifying the currents circulation and winds, reducing the freshwater inputs, increasing salinity and hypoxia, modifying the nutrient supply and ocean chemistry *(Yáñez et al., 2017)*. Moreover, a decrease in freshwater input, higher SST and salinity increase are favourable to harmful algal blooms (HABs) formation as Northern Patagonia has already experienced it during a drought in summer 2015-2016 *(León-Muñoz et al., 2018)* with economic loss estimated to US$200 million for salmon industry only *(Yáñez et al., 2017)*.

1.2 Marine heatwaves

1.2.1 Marine heatwaves in a global warming context

The first time the expression “marine heat wave” (MHW) has been used was in 2011 by Pearce et al. to describe a prolonged anomalously warm event off Western Australia in 2010-11. Since then, a new domain of study has emerged and MHWs are now studied as soon as they are occurring and retrospectively. MHW’s definition has been given by Hobday et al. in 2016: “MHW is defined as a portion of the ocean where SST exceeds the 90th percentile (based on a long-term climatology of at least 30 years) during at least 5 days with no more than 2 below-threshold days. A MHW can be described by its duration, intensity, rate of evolution and spatial extent”. The definition of the threshold and the climatology’s length are discussed in the part 5.1. According to that definition (moving threshold calculated depending on a climatology), severity of the MHWs depends on both absolute SST and on local seasonal SST variability. Consequently, a high temperature above the threshold does not always imply a

severe MHW.

Extreme warming events in the oceans have become more frequent over the years *(Oliver et al., 2018)*. Lima & Wethey (2012) estimated that between the 1980s and the 2010s, 38% of the world's coastal zones suffered from an increase of extremely warm SST events. More recently, the IPCC has estimated in 2021 that the frequency of MHWs has doubled since the 1980s and is believed to continue to increase, particularly in the coastal zones *(IPCC, 2021)*. For example, in 2015-2016, at least 1/4 of the oceans has experienced a MHW *(Oliver et al., 2017)*. Although it remains unclear how human-induced global warming is linked to MHWs, it has been shown that the number of impactful MHWs has increased because of human activities *(Laufkötter et al., 2020)*.

MHWs not only affect the surface of the oceans but also the subsurface. Indeed, MHWs can extend vertically over several tenths of meters *(e.g. Chen et al., 2021)*, sometimes superior to 100 m *(e.g. Pearce & Feng, 2013; Jackson et al., 2018; Su et al., 2021)*. Due to the higher thermic capacities of deep waters, while MHWs are dissipating in surface, warm-water anomalies can persist over several years at depth *(e.g. Jackson et al., 2018)*. However, few studies focus on the subsurface MHWs and for now little is known about it.

1.2.2 Creation, maintenance and consequences of marine heatwaves

In this section, we will assess a non-exhaustive review of the factors that can contribute to the formation and the maintenance of MHWs and what major consequences are observed following such events. Figure 5 summarizes the most iconic events that have occurred around the globe, their main drivers and consequences.

1.2.2.1 Atmospheric and oceanic factors inducing MHWs

Diverse factors, both atmospheric and oceanographic ones, with different time and spatial scales, can lead to ocean's mixed layer warming, inducing formation, maintenance and disappearance of MHWs *(e.g. Holbrook et al., 2019)*. However, although mechanisms that contribute to the formation of such events are becoming well known, the way they interplay to initiate and maintain MHWs remains uncertain. Most of the time, local and global processes (described below) act together to induce and maintain MHWs but can also act independently.

The principal factor triggering MHWs at mid and high latitudes is large-scale atmospheric pressure anomalies such as persistent high-pressure systems which can bring warm air, weaken the winds and might lead to reduced cloud coverage and precipitations *(e.g. Black et al., 2004; Holbrook et al., 2019; Sen Gupta et al., 2020)*. The combination of those factors

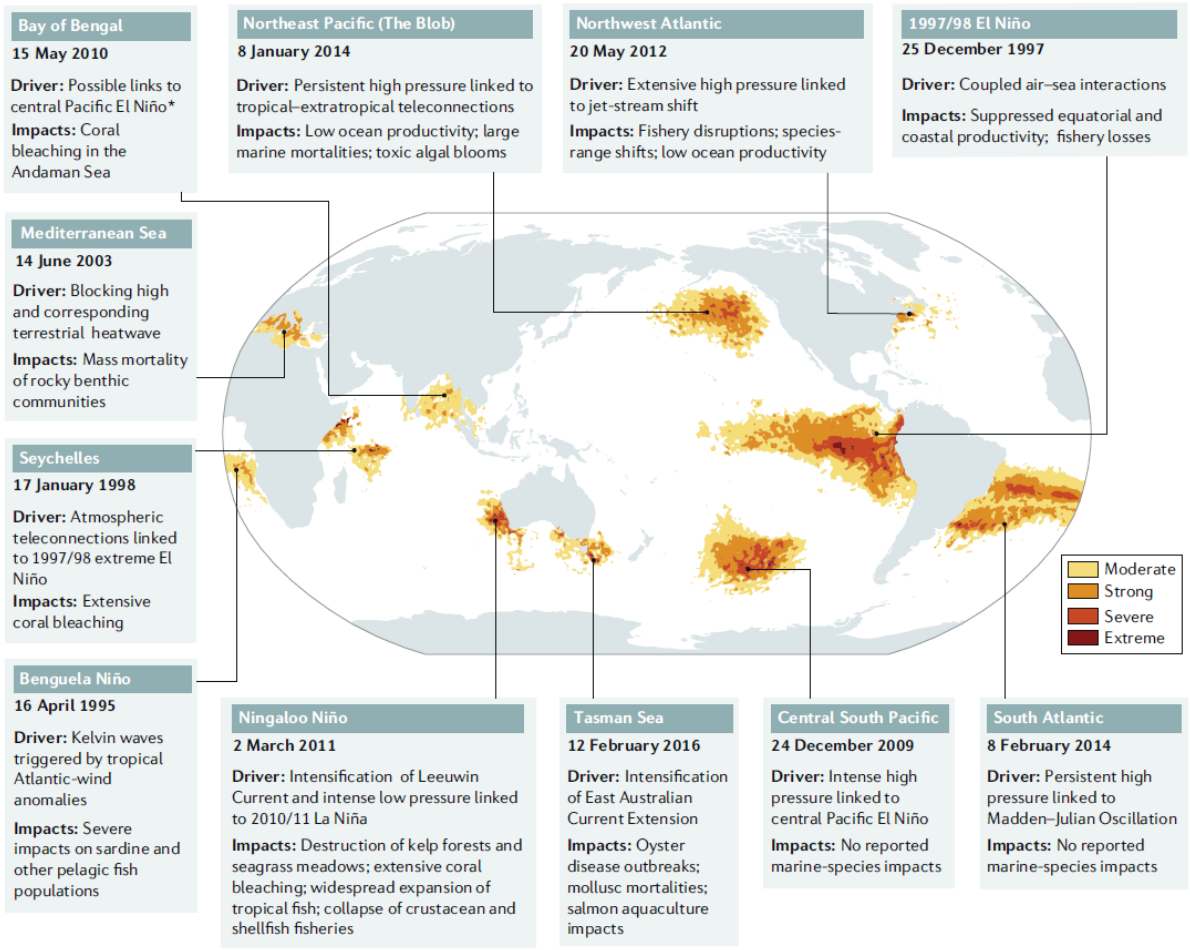

Figure 5: Drivers and main impacts on ecosystem of the major (since 1995) marine heatwaves (MHWs) events. The colour scale represents the intensity of the MHWs, "extreme" category representing the most intense MHWs events (see Hobday et al., 2018 or section 3.5.2). Figure by Holbrook et al., 2020

can lead to the reduction of heat transfer from the ocean to the atmosphere associated with reduction of turbulent mixing, favouring the sea surface warming *(Olita et al., 2007; Bond et al., 2015; Myers et al., 2018; Schmeisser et al., 2019; Sen Gupta et al., 2020)*. Sen Gupta et al. (2020) underlined that suppression of turbulent fluxes might be one of the main causes of MHW formation, whereas increase of turbulent fluxes might be the main cause of MHW dissipation. This combination of factors triggered, for example, the very long MHW in North Pacific Ocean in 2013-2015 *(e.g. Bond et al., 2015)* and the 2003 MHW in Western Mediterranean Sea which was besides enhanced by a continental heatwave *(Black et al., 2004; Schär et al., 2004)*. Local wind reduction or disappearance can also contribute to strengthening the MHWs (e.g. 2011 MHW in Western Australia, *see Benthuysen et al., 2014)*.

Oceanic processes, such as warm current advection, were also involved in the formation of several MHWs events *(e.g. Hobday et al., 2016; Holbrook et al., 2019; Oliver et al., 2021)*. Indeed, the incoming warm waters in colder areas (generally higher latitudes) lead to SST

anomalies and so to MHWs conditions, as it occurred for instance in 2011 in Western Australia where a MHW emerged because of warm current advection *(e.g. Benthuysen et al., 2014)*. On the contrary, the suppression of ocean advection can also cause MHWs as the water masses are "stagnant", reducing surface heat loss, as it occurred for 2013-2015 MHW in North Pacific Ocean *(e.g. Bond et al., 2015)*.

Direct increase of solar radiation, water stratification, local suppression of latent and/or sensible heat loss, and eddies instabilities are also processes inducing a diminution of heat loss from the ocean to the atmosphere and can induce and/or contribute to the maintain of MHWs *(Holbrook et al., 2019, 2020)*. Upwellings can also be a determinant factor by promoting the MHWs when upwellings are weaker than usual. On the contrary, upwellings can compensate for MHWs warming by bringing cool water to the surface *(Varela et al., 2021)*.

Retroactions from ocean to atmosphere may also contribute to the maintain of MHWs: positive SST anomaly might induce an augmentation of the air temperature, reducing the cloud coverage and weakening wind speed, initiating a positive thermodynamic feedback between atmosphere and sea *(Di Lorenzo & Mantua, 2016).* This positive SST-cloud feedback may play an important role in the maintenance of MHW at low-latitudes as the heat budget will be positively modified by a higher solar radiation *(Myers et al., 2018)*. Conversely, at mid-latitudes the positive SST-cloud feedback is not expected to have an impact on MHWs formation as the increase of solar radiation is compensated by a higher long wave radiation from the ocean to the atmosphere *(Schmeisser et al., 2019)*.

In addition to the factors cited above, remote sources have often played a major role, not only in MHWs formation but also in their maintenance. Indeed, propagation of planetary waves in the atmosphere or in the ocean can modify wind force or circulation, thermocline depth leading to the modification of local circulation by an increase or a reduction of currents advection, or modified the cloud coverage *(Holbrook et al., 2019)*. Sen Gupta et al. (2020) reported that the MHWs with the largest horizontal extent and the longest duration were associated with ENSO. For example, the 2011 MHW in Western Australia was induced by strong La Niña conditions, modifying the currents' circulation *(e.g. Pearce et al., 2011; Feng et al., 2013; Pearce & Feng, 2013)*, and the 2013-2015 MHW in Pacific Ocean was maintained and extent thanks to strong El Niño conditions *(e.g. Jacox et al., 2016)*.

1.2.2.2 MHWs' repercussions

Globally, the knowledge about MHWs consequences has been obtained through the

study of the major MHWs events. The studies of MHWs' consequences mainly focus on species and ecosystem health, especially on emblematic species or ecosystems such as kelp forests or coral reefs, and on how MHWs may alter fishing catches and aquaculture farming.

However, all species are not affected in the same way by MHWs. For mobile species, the migration is possible and can be either latitudinal (poleward) or vertical (deepward) and has been observed for multiple species *(e.g. Deutsch et al., 2015; Rutterford et al., 2015; Barange et al., 2018)*. Two types of migration are possible: forced migration to escape thermal stress and/or starvation *(e.g. Mills et al., 2013)* or opportunist migration with warm-water species taking advantages of warming SST to extend their geographical range *(e.g. Wernberg et al., 2013; Lonhart et al., 2019; Miyama et al., 2021).*

Sessile or sedentary organisms such as corals, seagrass meadows, eels or various invertebrates, are much more vulnerable to MHWs as they cannot migrate *(e.g. Pearce et al., 2011).* For them, MHWs may led to their habitat reduction over temporary or long-term period *(e.g. Smale & Wernberg, 2013)*, genetic loss *(Deluqui-Gurgel et al., 2020)*, genetic tropicalization *(Coleman et al., 2020)*, failure in reproduction *(e.g. Thomson et al., 2015)* or to mass mortality. Mass mortality during MHWs can be induced by both direct and indirect factors, such as thermal stress leading to organisms' death *(Garrabou et al., 2007; Pearce et al., 2011; Thomson et al., 2015; Couch et al., 2017; Oliver et al., 2017)*, or modifications in the food-chain assemblage, resulting in species shifts and starvation of the upper trophic levels *(Welch, 2015; Cavole et al., 2016; Barbeaux et al., 2018)*. Indeed, starvation has been often linked to MHWs because of a diminution of the lower trophic levels; for instance, 72% of the events have been associated with low chlorophyll-*a* concentrations *(Sen Gupta et al., 2020)*. In addition, major shifts in ecosystems communities have been observed following a MHW. Indeed, coral reefs and seagrass meadows, forming rich ecosystems *(Reaka-Kudla, 1997; Morrison et al., 2014)*, were often hit by MHWs, resulting in coral bleaching and massive seagrass meadow dieback *(e.g. Le Nohaïc et al., 2017; Dalton et al., 2020; Filbee-Dexter et al., 2020; McPherson et al., 2021)* and then in shifts in the ecosystems assemblages *(e.g. Arafeh-Dalmau et al., 2019)*.

Not only affecting natural habitats, MHWs have also strongly affected fisheries and aquaculture. Indeed, it has been shown that MHWs are exacerbating global change impacts on fisheries *(Cheung & Frölicher, 2020)*. Species communities shifts, migrations and mass mortality have seriously reduced fishing captures following strong and/or long MHW *(e.g. Caputi et al., 2016; Barbeaux et al., 2018; Barbeaux et al., 2020)*. In addition, the latitudinal

migration of some species, such as higher trophic level predators, have caused competition with fisheries *(e.g. Santora et al., 2020; Tanaka et al., 2021)*. Nonetheless, MHWs had also positive impacts on fisheries, as the migration of commercial species closer to the coasts were observed, allowing higher than usual captures *(Cavole et al., 2016; Santora et al., 2020; Miyama et al., 2021)*. In some cases, recreational fishing has also been favourited by MHWs as recreational fishermen's appreciated species were much caught thanks to the warmed waters *(e.g. Oliver et al., 2017)*. Regarding aquaculture, different MHWs were reported as devastating for farming. Indeed, with no way to migrate, species are highly vulnerable to the warming waters, resulting in cessation of food intake, reduced growth due to thermal stress, and in the worst case to mass mortality *(e.g. Pearce & Feng, 2013; Oliver et al., 2017; Wade et al., 2019).*

On top of that, it has been shown that MHWs favour environment's conditions to HABs development by increasing water temperature and stratification, causing among others mass mortality *(e.g. Roberts et al., 2019)* and changes in migration routes *(e.g. Santora et al., 2020)*. When occurring near aquaculture farms, HABs cause large damages and may facilitate the spreading of viruses *(Green et al., 2014; NOAA Climate, 2015; Oliver et al., 2017)*, impacting humans' economy by leading to delayed fishing season *(Mills et al., 2013)*, closure of hatcheries and shellfish harvest *(Di Lorenzo & Mantua, 2016; McCabe et al., 2016)*, closure of recreational and commercial fishing, inducing million dollars economic loss *(Cavole et al., 2016)*.

In addition to direct biological consequences, MHWs have also been reported for their impacts on the ocean's biogeochemistry, but those repercussions are much less studied. For instance, by increasing the stratification, MHWs can lead to a reduced influx of nutrient in the surface layer *(e.g. Smale et al., 2019)* or reduce the oxygen dissolution and even in some conditions lead to anoxic waters *(e.g. Brauko et al., 2020)*. In other cases, MHWs may modify the carbon cycle by reducing ocean carbon intake *(Mignot et al., Preprint)* or by releasing in the atmosphere the carbon which was stored in the oceans, for example when large-scale seagrass meadows diebacks are provoked *(Arias-Ortiz et al., 2018)*.

In addition to all precedent repercussions that MHWs may have, modification in the sea ice formation has been observed for MHWs occurring in the Arctic Ocean by preventing water cooling *(Hu et al., 2020; Carvalho et al., 2021)*. Moreover, it has been shown that MHWs could influence coastal urban areas by modifying the air moisture and temperature *(Hu, 2021)*.

2 OBJECTIVES OF THE MASTER'S THESIS

Given the increasing duration, intensity and frequency of MHWs and given the huge impacts they have on ecosystems and biogeochemical cycles, affecting human fisheries and oceanic farming, MHWs have drawn researchers' attention over the last few years. Though, although the phenomena leading to MHWs formation are becoming well-known, the way they interact together remains not fully understood and differs from one event to another. Moreover, as the phenomenon is becoming more intense, we can expect that its consequences will be more devastating with the years, justifying the need for a deeper understanding of the MHWs occurring all around the globe.

Central and South Chile (29°S-55°S), supporting large aquaculture farming based on relatively cold-water species, is already facing global change effects in the form of drought, modifications of large-scale forcings, toxic blooms, reduced river inputs and hypoxic tendencies. According to these criteria, this part of Chile should be highly vulnerable to the MHWs occurrence. However, to the best of our knowledge, MHWs have never been studied yet in these regions.

Therefore, the first objective of this master thesis is to realise a global assessment of the MHWs that have occurred off Central and South Chile over the last 4 decades (1982 to 2020).

The second objective is to analyse the metrics of those MHWs, such as the number of events per year, their duration and their average and maximal intensity, in order to determine when the most important events occurred and if long-term trends can be observed. In addition, decadal trends of the MHWs' metrics will also be assessed. As a complement, we will perform analysis of the spatial long-term trends of both SST and MHWs frequency over the last 40 years to know which regions might be affected by warming trends and increasing MHWs frequency. Decadal SST trends will also be addressed to know if one decade has particularly suffered from the global warming trends.

The third objective of this work is to have a better understanding of the factors that contribute to the formation of MHWs events along Chilean coasts and to understand how they interplay. For that point, we will focus our study on the comprehension of the formation of successive unusually long and severe MHWs events that have occurred during the year 2016. We will assess how oceanic, atmospheric and remote forcings (ENSO and SAM) have led to the formation of such events and how they are related.

3 MATERIEL ET METHODES

3.1 Studied area

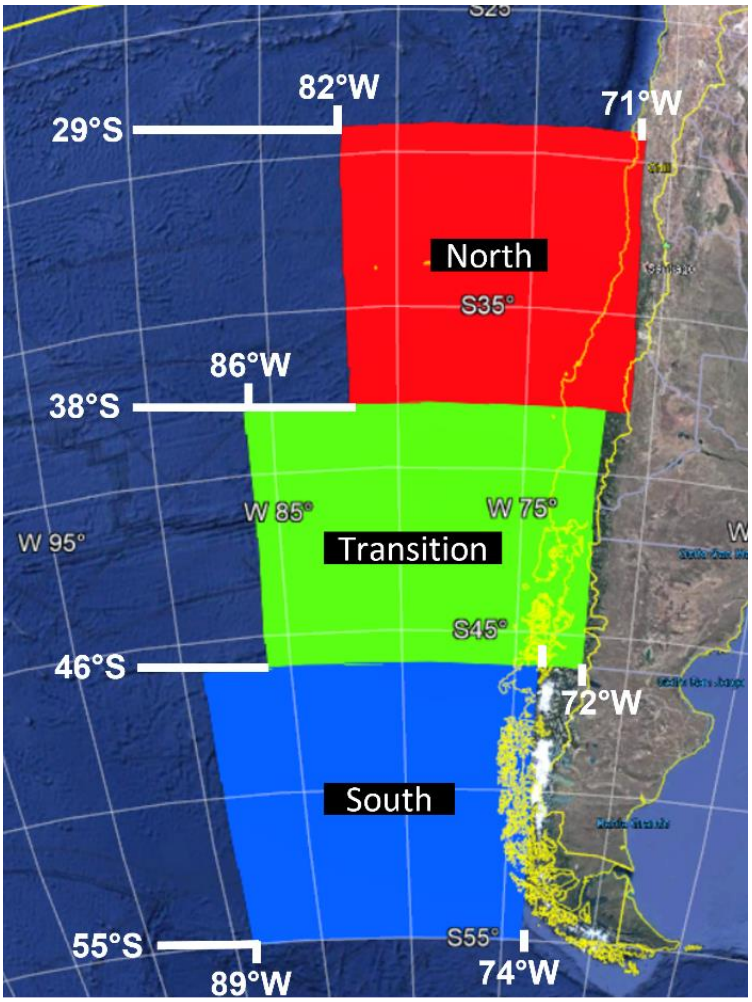

Figure 6: Studied areas. In red: Northern area (-82°E to -71°E and 38°S to 29°S); in green: Transition area (-86°E to -72°E and 46°S to 38°S); in blue: Southern area (-89°E to -74°E and 55°S to 46°S).

In this study, we will focus on the Southeastern Pacific Ocean, along the Central and Southern Chile, from 29°S to 55°S, separated in 3 distinct zones (Figure 6). Strub et al. (2019) defined a "transition zone" between 38°S and 46°S where the Westerly Winds and the South Pacific Current alternate from equatorward direction in summer to poleward in winter (see details in part 1.1.2.2). Therefore, this transition zone, encompassing the Northern Patagonia, will constitute our central studied area. We defined two other areas, the first being the Southern Patagonia, 46°S to 55°S (we did not consider south of 55°S as the Antarctic Circumpolar Current is becoming strong south of this latitude; *Orsi et al., 1995*). We will refer to this zone as the "Southern area". The second one is north of the Transition Area, from 29°S to 38°S, corresponding to Central Chile, named in this study the "Northern area". Longitudinally, the

areas were delimited in order to have a similar oceanic surface. Northern area is limited from -82°E to -71°E; Transition area from -86°E to -72°E; Southern area from -89°E to -74°E.

In each one of the 3 areas, we will calculate MHWs occurrence and metrics associated and, in further steps, determine the phenomena that have led to MHWs formation.

3.2 Data

3.2.1 Oceanic data

A part of our studied area is located at relatively high latitudes, where cloud coverage is high. Therefore, we decided to not use infrared satellite data, which has a high resolution but interferes with clouds. Instead, we used daily microwave satellite data from Advanced Microwave Scanning Radiometer 2 instrument, abbreviated AMSR-2 (from Global Change Observation Mission satellite, also named GCOM-W1, available at http://www.remss.com), as they do not interfere with clouds. This data has a spatial resolution of 1/4 degree and has been downloaded for the entire South Pacific Ocean for the whole available period, which means from 2012-07-03 to 2020-12-31. However, microwaves interfered with rain; thus, satellite data are still incomplete. Reconstruction of the SST field was performed with DINEOF tool and described in section 3.3.

SST anomalies were calculated by doing the difference between reconstructed SST data and daily long-term average. The long-term average has been calculated with daily-resolution Optimum Interpolated Sea Surface Temperature (OISSTv2) provided by NOAA (available at https://psl.noaa.gov/data/gridded/data.noaa.oisst.v2.highres.html). OISSTv2 is one of the longest temporal global SST data available and allows to have almost 40 years of daily data with a spatial resolution of 1/4 degree. Therefore, we downloaded the data over the whole period available at the moment, that is to say from 1982 to 2020.

OISSTv2 SST data was also used to calculate the long-term climatology for the MHWs detection and the MHWs detection itself. In addition, we used this dataset to calculate SST long-term trends (described in part 3.4).

3.2.2 Atmospheric data

3.2.2.1 Pressure, atmospheric temperature and winds

Sea level pressure, 2 meters above surface air temperature and zonal and meridional winds components 10 meters above surface were studied from 1982 to 2020 using the European Centre for Medium-Range Weather Forecast (ECMWF) reanalysis data (ERA5; see Table 1)

available at https://cds.climate.copernicus.eu/#!/home. Daily and monthly average atmospheric temperature anomalies were calculated using the data described above doing respectively the difference between daily and monthly air temperature and long-term daily and monthly mean from 1982 to 2020. Same for daily and monthly sea level pressure anomalies.

Winds were analysed over the period 2012 to 2020 (hourly temporal resolution) and wind speed (ws) was calculated from u and v component (respectively eastward and northward components) following this equation:

$$ws = \sqrt{u^2 + v^2}$$

Time series of atmospheric temperature, sea level pressure, winds and anomalies for both atmospheric pressure and temperature were also calculated and a 3-months Gaussian filter was applied on each variable to abstract variability inferior to the season.

Table 1: Details about the different datasets used for atmospheric analysis.

Data provider	Dataset	Product type	Variable	Units	Spatial resolution	Temporal resolution
ECMWF	ERA5	Reanalysed product	Atmospheric temperature	°C	1/4 degree	Daily
ECMWF	ERA5	Reanalysed product	Sea level pressure	hPa	1/4 degree	Daily (to calculate anomalies) and Hourly
ECMWF	ERA5	Reanalysed product	Surface net solar radiation	W/m²	1/4 degree	Hourly
ECMWF	ERA5	Reanalysed product	Surface sensible heat flux	W/m²	1/4 degree	Hourly
ECMWF	ERA5	Reanalysed product	Surface latent heat flux	W/m²	1/4 degree	Hourly
ECMWF	ERA5	Reanalysed product	Surface net thermal radiation	W/m²	1/4 degree	Hourly
ECMWF	ERA5	Reanalysed product	Wind (U and V components)	m/s	1/4 degree	Hourly
ECMWF	ERA5	Reanalysed product	Forecast albedo	Dimensionless	1/4 degree	Hourly

ECMWF	ERA5	Reanalysed product	Low cloud coverage	Dimensionless	1/4 degree	Hourly
ECMWF	ERA5	Reanalysed product	Total cloud coverage	Dimensionless	1/4 degree	Hourly

3.2.2.2 Heat fluxes

The heat fluxes were calculated from 2012 to 2020 to understand if they were involved in the formation or maintenance of MHWs. They are calculated as follow:

$$Qi = Qs - Qb - Qe - Qc$$

where Qi is the total net heat flux at the surface of the ocean, Qs the surface net solar radiation (also known as shortwave radiation) that reaches a horizontal plane at the surface of Earth minus what is reflected by Earth's surface (governed by the albedo); Qb is the surface net thermal radiation (also known as longwave radiation) which is the difference between downward and upward radiation received/emitted by Earth's surface; Qe is the surface latent heat flux representing the transfer of latent heat (e.g. heat transfer due to evaporation or condensation) between atmosphere and Earth's surface through turbulent motion; Qc is the sensible heat flux, i.e. the heat transfer between Earth's surface and atmosphere via turbulent motion but not taking into account heat transfer resulting from water phase change (e.g. evaporation and condensation). In addition, we also had a look at the albedo pattern which is the reflectivity of the Earth's surface, the low cloud coverage which is the portion of clouds in the lower levels of the troposphere and the total cloud coverage through the entire atmosphere.

To evaluate heat fluxes, albedo and cloud coverage, we used ECMWF's products (described in Table 1) over the period 2012 to 2020.

We have calculated a spatial average of the heat fluxes between the ocean and the atmosphere within the 3 studied areas (Northern, Transition, Southern areas) to know the temporal evolution and applied a 3-month Gaussian filter to subtract variations inferior to seasons. Time series of albedo and cloud coverage were also calculated by doing the spatial average within the 3 studied areas. We also calculated heat fluxes monthly averaged from 2012 to 2020 with the same data used above. In addition, we calculated the anomaly of the total heat transfer from the ocean to the atmosphere ($Qbec$), which is the sum of Qb, Qe and Qc, by subtracting $Qbec$ monthly climatological mean (calculated based on 2012 to 2020 values) from monthly averaged $Qbec$ values.

Within this study, we will consider that fluxes from ocean to the atmosphere are heat

loss from the ocean, i.e. negative fluxes, whereas fluxes from the atmosphere to the ocean are heat gain for the ocean, i.e. positive fluxes.

3.2.2.3 Remote forcings

Different remote forcings were evaluated (details in Table 2). For ENSO, we used the Oceanic Niño Index (ONI) provided by NOAA to monitor El Niño and La Niña phases. This index indicates the difference between the 3-month running mean SST and the 30-year climatology in the tropical Pacific between 120°-170°W (Niño3.4 region). El Niño (La Niña) phases are determined when the index is above (below) +0.5 (-0.5). For PDO, we used the ERSST PDO index provided by NOAA. It is the dominant year-round pattern of monthly SST anomalies in the Northern Pacific obtained via empirical orthogonal function analysis. For SAM, we used the index calculated according to Marshall's method (2003) expressing the zonal pressure difference between 40°S and 60°S.

All indexes were analysed from 1982 to 2020. We applied a 3-month Gaussian filter for PDO and SAM but not for ONI as it is already calculated as a 3-month average.

Table 2: Large-scale remote forcings indexes.

Index	Full name	Data provider
ONI	Oceanic Niño Index	NOAA https://origin.cpc.ncep.noaa.gov/products/analysis_monitoring/ensostuff/ONI_v5.php
PDO index	Pacific Decadal Oscillation Index	NOAA https://www.ncdc.noaa.gov/teleconnections/pdo/
SAM index	Southern Annular Mode Index	Gareth Marshall https://legacy.bas.ac.uk/met/gjma/sam.html

3.3 Reconstruction of the SST field

Data INterpolating Empirical Orthogonal Functions (DINEOF) was used to reconstruct the blanks in the SST field. It is a tool developed by Beckers and Rixen (2003) and based on an empirical orthogonal functions (EOF) calculation enabling to fill blanks in large sets of data, especially satellite ones *(Alvera-Azcárate et al., 2005)*. To fill the missing data, first, DINEOF removes a spatial and a temporal mean to the original dataset, and the missing data are set to zero. Then, a first EOF decomposition is performed with the first EOF for this field and the missing values are replaced by the values obtained by this EOF decomposition. In parallel, DINEOF calculates a cross-validation error. Then, the EOF decomposition and error calculation

are repeated with 2 EOFs, then 3 EOFs, etc. The final number of EOFs retained corresponds to the minimal error obtained by the cross-validation. DINEOF has been applied year by year to fill the blanks in order to avoid working with too large data files.

DINEOF reconstruction was validated by calculating the bias, correlation and root mean square error (RMS) between the reconstructed field and the in situ data. We used drifting buoys present in our studied area at different time periods. The buoys data are available at https://map.emodnet-physics.eu/. We used 10 drifting buoys with hourly temporal resolution, all scattered offshore Central and South Chile between the coast and about 2 500 km offshore, with a complete temporal coverage from 2014 to 2020. In total, 4219 points were used to estimate the accuracy of our reconstruction. Validation of the SST reconstruction and the reconstruction itself are shown in the Results.

3.4 SST trends

We calculated the seasonal mean SST over the studied area by doing the long-term average (1982 to 2020) over austral summer, autumn, winter and spring.

To calculate the SST long-term trends, as a first step we removed SST seasonal variation to our SST values through a low-pass filter in order to have only the annual SST trends and abstract seasonal variations. Then, SST linear trends were calculated from 1982 to 2020, by using the OISSTv2 dataset (described in part 3.2.1). Linear trend by least-square is calculated thanks to the tool "trend" developed by Greene et al. (2019) which is part of the Climate Data Toolbox for MATLAB. The significance of the trend is estimated by the p-value, also given by this tool. We choose p-value inferior to 0.05 as a significant trend to be in adequation with the MHWs significative trends (part 3.5.1). Secondly, trend calculation was performed again over ten-year periods, from 1982 to 1991, 1992 to 2001, 2002 to 2011 and 2012 to 2020.

3.5 Marine heatwaves

3.5.1 Definition and detection of marine heatwaves

In this study, we used the MHW definition given by Hobday et al. (2016), which defines MHWs as continuous events of warm SST anomalies exceeding a threshold (90^{th} percentile with respect to a 30-years climatology) during at least 5 days. Our marine heatwave detection is based on the HeatWaveR algorithms provided by Schlegel and Smit in 2018 (R language, available at https://robwschlegel.github.io/heatwaveR/index.html). It is the translation of Python algorithms originally written by Hobday et al. (2016). This algorithm is able to determinate when MHWs are occurring, calculating for each day a long-term climatology, a

threshold according to this climatology (90th percentile), and find the periods during which SST exceed this threshold during at least 5 days with no more than 2 below-threshold consecutive days, based on a 11-days moving mean centred on each Julian day (in the case of time series SST data) or on each pixel (in the case of gridded data).

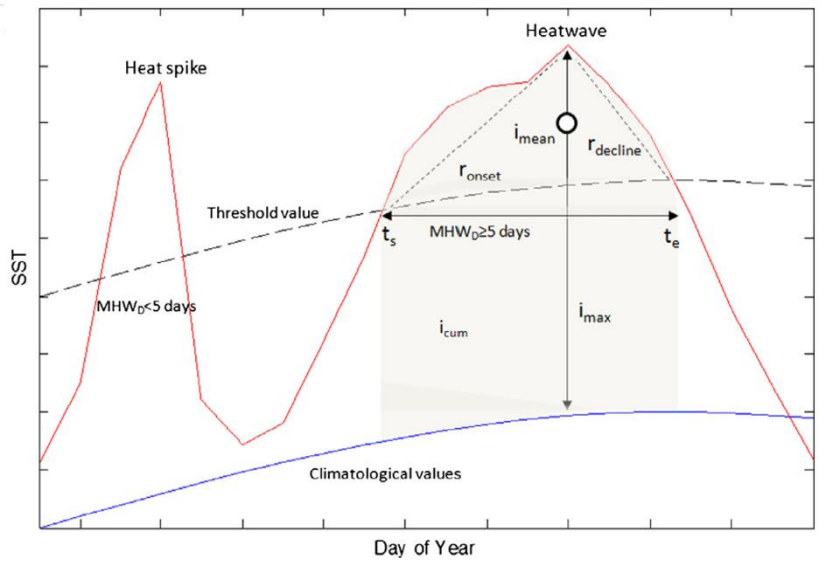

Figure 7: Representation of how are defined marine heatwaves (MHWs) and MHWs' metrics. Threshold values (dashed line) is based on the 90th percentile of a long-term climatology (blue line). The heat spike represents an above threshold period with a duration inferior to 5 days (thus not a MHW). MHW duration (MHW_D) is the time period between the beginning of the MHW (t_s) and its end (t_e). Maximal intensity (i_{max}), rate of temperature increase (r_{onset}) and rate of temperature decline ($r_{decline}$) are defined according to the MHW's highest peak. The mean event intensity (the white circle; i_{mean}) is the MHW's mean intensity and the cumulative intensity (grey shaded area; i_{cum}) is the sum of daily intensities during the MHW. Hodbay et al., 2016

In addition to the MHW calculation, the algorithm provides several metrics: number of events per year, duration of each event, maximal, mean and cumulative intensity, onset and decline rate (Figure 7; Table 3). However, in this study we will only focus on the primary metrics (i.e. number of events per year, duration of each event, maximal and mean intensity).

Table 3: Definition of the metrics used to define a MHW. Adapted from Hobday et al., 2016.

	Name	Definition	Units
Primary	Climatology	T_m: The climatological mean, calculated over a reference period, to which all values are relative	°C
	Threshold	The seasonally varying temperature value that defines a MHW (e.g. T_{90} is the 90th percentile value based on the baseline periods)	°C
	Start and end of the MHW	t_s, t_e: dates on which a MHW begins and ends	Days
	Count	Number of events per year	

	Duration	D: Consecutive days during which temperature exceeds the threshold	Days
	Intensity (max/mean)	i_{max}: highest temperature anomaly value during the MHW i_{mean}: mean temperature anomaly during the MHW	°C
Secondary	Rate measures	r_{onset}: rate of temperature change from the onset of the MHW to the maximum intensity $r_{decline}$: rate of temperature change from the maximum intensity to the end of the MHW	°C/day
	Cumulative intensity	i_{cum}: sum of daily intensity anomalies. Note that the integral omits t_e which is below the T_{90} threshold	°C.days

To calculate the climatology, Hobday et al. (2016) preconize to have at least 30 years of SST data because multi-year cyclic events (e.g. ENSO) must be considered to calculate MHWs. Here we used the same dataset as they did, that is to say the OISSTv2 dataset but over a longer period, from 1982 to 2020. The threshold we used to calculate MHWs is the 90th percentile.

Moreover, the algorithm also determines the long-term trends in MHW occurrence by first calculating the number of MHW in each pixel of the gridded data that has occurred, in our case between 1982 and 2020, and then applying a generalised linear model to each pixel. From the generalised linear model, slope and p-value (<0.05) are used to determine the long-term trends in MHW occurrence.

3.5.2 Classification of marine heatwaves

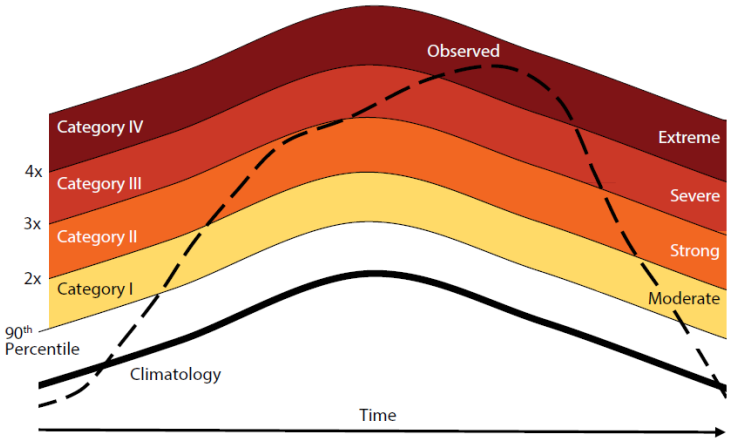

Figure 8: Schematic explanation of how marine heatwaves (MHWs) can be categorized. The bold line represents the long-term climatology at one place, dashed line represents the observed temperature at the same place. The first thin black line separating no MHW and category I MHW represents the 90th percentile (the threshold). In this case, the observed temperature peaked above 4 times the difference between the climatology and the threshold, meaning it is a Category IV MHW (extreme event). Hobday et al., 2018

Hobday et al. (2018) have proposed a classification of the MHW events in order to understand the real impact of the MHWs on ecosystems and to have more visual elements for scientific communication. This classification has 4 categories which depend on the maximal intensity reached by the MHW event (which in turn depends on the climatology; Figure 8). Categories are based on multiples of the local difference between the climatology and the threshold (Table 4). This categorization is also given by the heatwave detection algorithm.

Table 4: Categorization of marine heatwaves, according to Hobday et al., 2018

Multiple of the difference between climatology and threshold	**Category**	**Intensity of the MHW**
0 to <1	No MHW	No MHW
1 to <2	Category I	Moderate
2 to <3	Category II	Strong
3 to <4	Category III	Severe
> 4	Category IV	Extreme

4 RESULTS

4.1 SST reconstruction

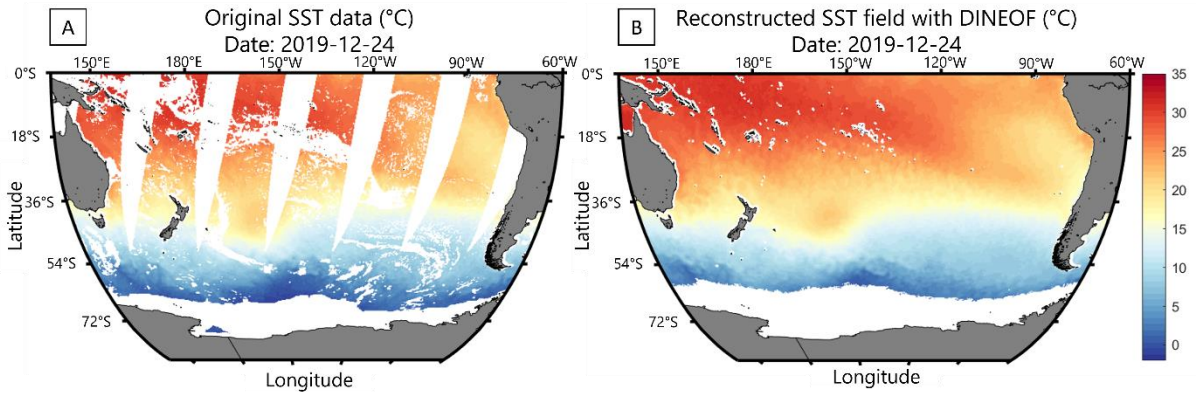

Figure 9: (Left) AMSR-2 sea surface temperature (SST; °C). White parts indicate the missing data due to rain, ice and satellite limitations (swaths). (Right) Reconstructed SST (°C) with DINEOF. Missing data are still present alongshore and everywhere water was covered at least one day by sea ice

AMSR-2 instruments measure the microwave radiation emitted from the ocean to measure SST. As microwaves interfered with rain, there is no data where rainy conditions are observed. Moreover, there is no data between the satellite's swaths and where ice is present (Figure 9A). As rain episodes and satellites' swaths are not fixed in time, DINEOF is able to fill the blanks. Nevertheless, nearshore data is never available because of the coarse resolution and due to land contamination, therefore, DINEOF reconstruction is impossible nearshore resulting in a band without data of 1/4° wide from every shore (Figure 9B). In addition, we decided that every portion of water covered at least one day by sea ice will not be part of the reconstruction, as we are not interested in high latitudes. For each year, the percentage of missing data in the original dataset for the whole South Pacific was between 35% and 37%. For the reconstruction, DINEOF has calculated 50 EOFs for each year, explaining in average 99.89% of the initial variance.

To estimate the accuracy of DINEOF reconstruction, we used in situ data from drifting

Table 5: Bias (°C), correlation and root mean square error (RMS, °C) calculated between original satellite SST and SST from in situ buoys and between the reconstructed SST field with DINEOF and the SST from the buoys. The number of points used for the reconstruction differs as there were missing data in the original satellite SST.

	Number of points	Bias (°C)	Correlation	RMS (°C)
Original data vs. buoys	3004	-0.06	0,98	0,55
Filled data vs. buoys	4219	-0.10	0,98	0,47

buoys. Correlation and root mean square error were calculated between in situ SST and original AMSR-2 satellite SST but also between in situ SST and DINEOF-reconstructed SST. Results are shown in Table 5. The number of points used for the calculation is also shown and differs as the original data is unfilled. The negative bias indicates that the satellite and the reconstructed SST are lower than the in situ SST. The bias, the correlation and the RMS are very close for both set of data, meaning that our reconstructed field is as accurate as the satellite data. Our reconstructed SST field can therefore be trusted.

4.2 SST variability

For the Northern and Transition areas, from 2012 to 2020, the SST is always higher than the air temperature (Figure 10). For the Southern area, the SST remains most of the time higher than the air temperature, particularly in winter, but during summer, the air temperature might surpass the SST during a few weeks. However, when the air temperature is higher than the SST, the difference remains very low (inferior to 0.5°C).

Seasonal variations of the SST are much more important in the Northern and Transition areas, which are constrained by the seasonal North-South variations of the SPSA and Westerly Winds (see part 1.1.2.2 for details). Indeed, for those two areas, there is a difference in the SST of about 5°C between winter and summer, with SST values ranging from 14°C in winter to almost 19°C in summer in the Northern area and from 10.5°C in winter to 15.5°C in summer for the Transition area (Figure 11). On the contrary, the SST in the

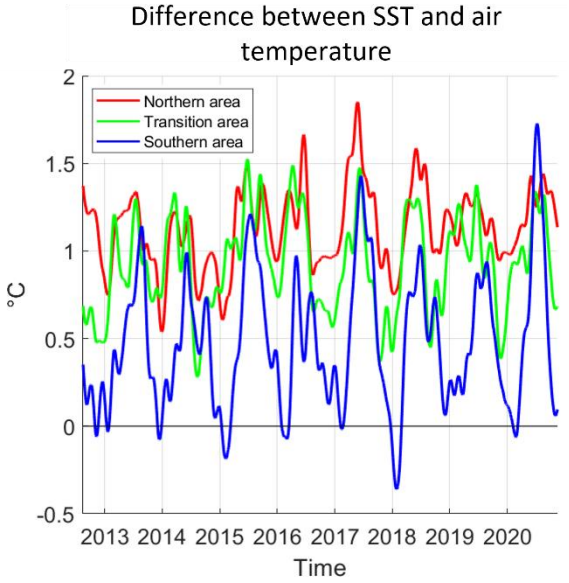

Figure 10: Difference between SST and air temperature (°C) between 2012 and 2020 for the Northern (red), Transition (green) and Southern (blue) areas. A 3-month Gaussian filter has been applied to smooth the results.

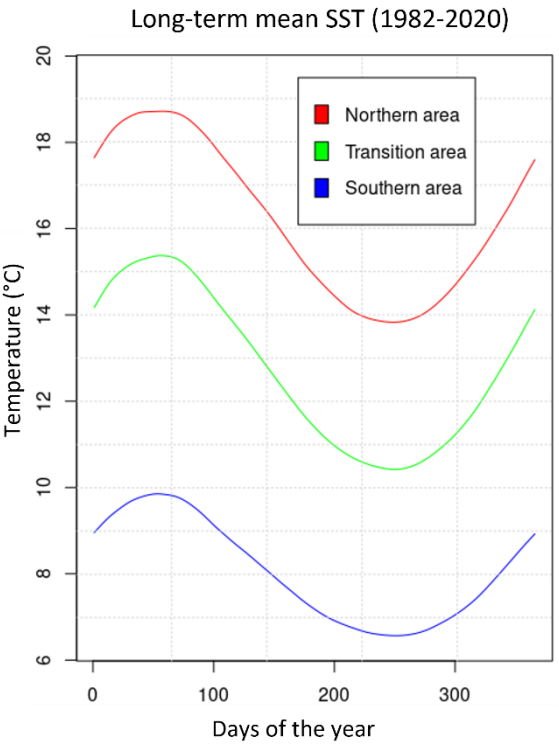

Figure 11: Long-term (1982-2020) mean SST for the Northern (red), Transition (green) and Southern (blue) areas. Those climatologies are used to calculate the SST anomalies and the MHWs.

Southern area has a lower seasonality with SST ranging from about 6.5°C in winter to 10°C in summer. Because of the variability, the threshold over which an event is classified as a MHW is different from one area to another one. For example, the threshold is highest for the Northern and Southern areas during summer, being about 1°C above the climatology, and is reduced in winter being about a half of degree above the climatology. On the contrary, in the Transition area, seasonal variability of the threshold is quite low, being about two thirds of degree above the climatology in summer and a half a degree above in winter.

4.3 Marine heatwaves in Central and South Chile: 40 years of data

To understand how MHWs have evolved within an almost 40 years period, we performed an analysis of the duration and intensity for each event and studied the number of MHWs occurring each year. We also studied MHWs decadal trends for the same variables.

4.3.1 Frequency of marine heatwaves

From 1982 to 2020, a total of 75, 73 and 71 MHWs events occurred, from which 5, 6 and 9 events had a duration superior to one month respectively in Northern, Transition and Southern area. In the Northern and Transition areas, the highest number of MHWs was recorded during one of the strongest El Niño events, respectively 9 in 1997 and 7 in 1998 (Figures 12A and 12B). For the Southern area (Figure 12C), there is no year during which the number of MHWs was particularly high in comparison to the other years, but in both 1987 and 2020, 6 MHWs were recorded (Figure 12C). For the Transition area, alternance of years with and without MHWs was common until 2011 (Figure 12B). Nonetheless, from 2011 to 2020, MHWs were recorded every year totalling 45% of all MHWs recorded for the area. The decade 2012-2020 was particularly significant in terms of number of MHW events for the Transition area, totalling on average twice more events than during the 1982-1991 decade and was 2.5 times superior to the number of events that have occurred during 1992-2001 and 2002-2011. It

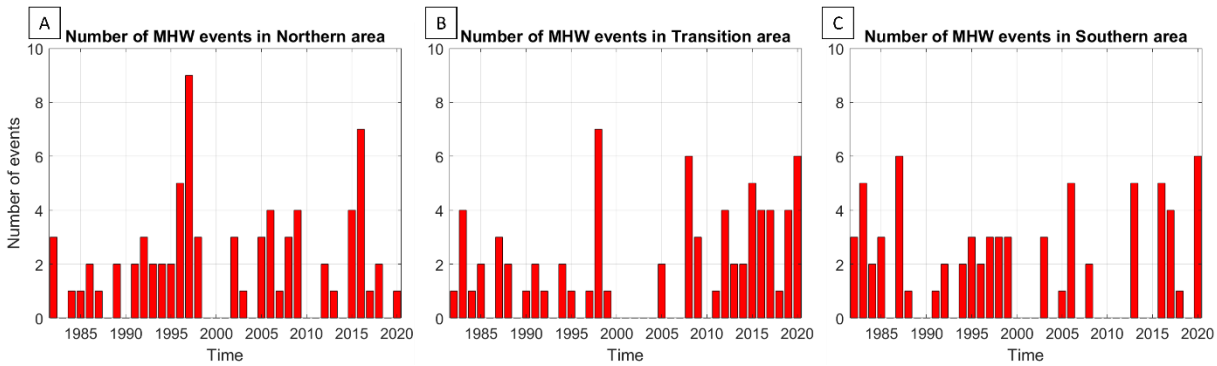

Figure 12: Number of marine heatwave events (MHW) that have occurred each year from 1982 to 2020 for Northern (left), Transition (central) and Southern (right) areas.

is notable that the early 21st century was MHWs-free for all 3 areas, and particularly for the Transition one.

4.3.2 Duration of marine heatwaves

For all 3 areas, the mean duration of MHWs for the 1982-1991 decade was about 10 days and was the lowest of the four decades (Figure 13A), whereas mean duration during the

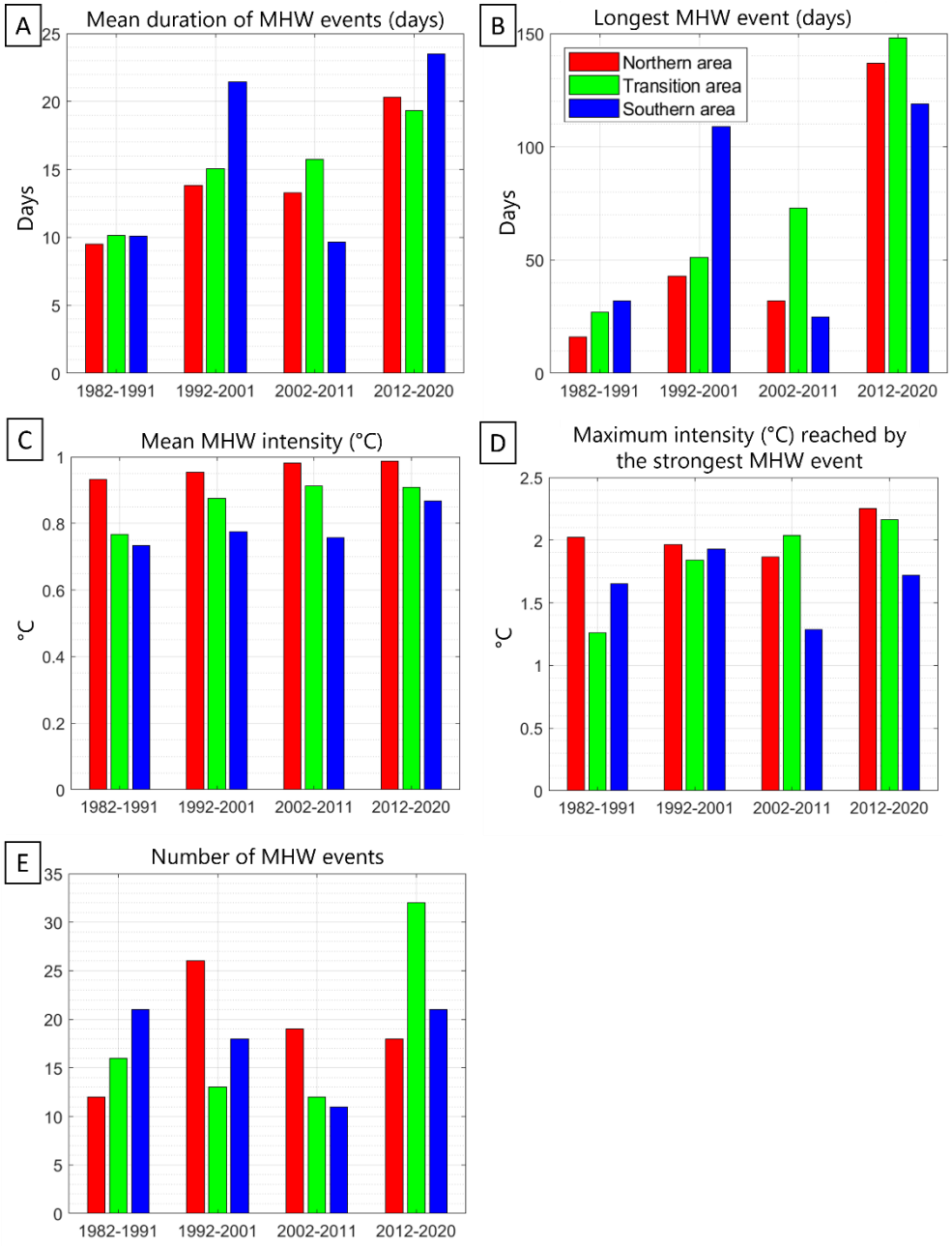

Figure 13: Decadal trends (1982-1991, 1992-2001, 2002-2012, 2012-2020) for Northern (red), Transition (green) and Southern (blue) areas. Parameters analysed over the different decades are: (A) mean duration (days) of the events that have peaked during the decade, (B) duration (days) of the longest event of the decade, (C) mean intensity (°C) of all the events that have occurred during the decade, (D) maximal intensity (°C) reached by the strongest event of each decade, (E) number of MHW events that have occurred throughout the decades.

2012-2020 decade was the longest recorded, with 20 days, 19 days, 23 days for respectively Northern, Transition and Southern area (Figure 13B). The mean duration was multiplied by 2.14, 1.9 and 2.3 respectively between the two decades. Between 1982-1991 and 2012-2020, the duration of the longest event has been multiplied by 8, 5 and 3 for respectively Northern, Transition and Southern areas.

In the Northern area, only one MHW had a duration superior to 2 months. This event was particularly long and lasted for 137 days (4.5 months), beginning in January 2017. The second longest one lasted for 43 days only and began in June 1998 (Figure 14A). In the Transition area, the longest event occurred in 2016, beginning in May, and lasted for 148 days (almost 5 months). Two other events greater than 2 months occurred, one beginning in January 2008 and lasting for 73 days, and the other one beginning in October 2016 and lasting for 64 days (Figure 14B). In the Southern area, the longest event began in June 2016 and lasted for 119 days (almost 4 months). Two other events had a duration superior to two months, both during 1998, the first one began in February and lasted for 99 days and the second one, beginning only 6 days after the dissipation of the previous event, in May, lasted for 109 days (Figure 14C). It seems important to highlight that only a few events had a duration superior to 1 month: 5, 6 and 9 events respectively for Northern, Transition and Southern areas.

4.3.3 Intensity of marine heatwaves

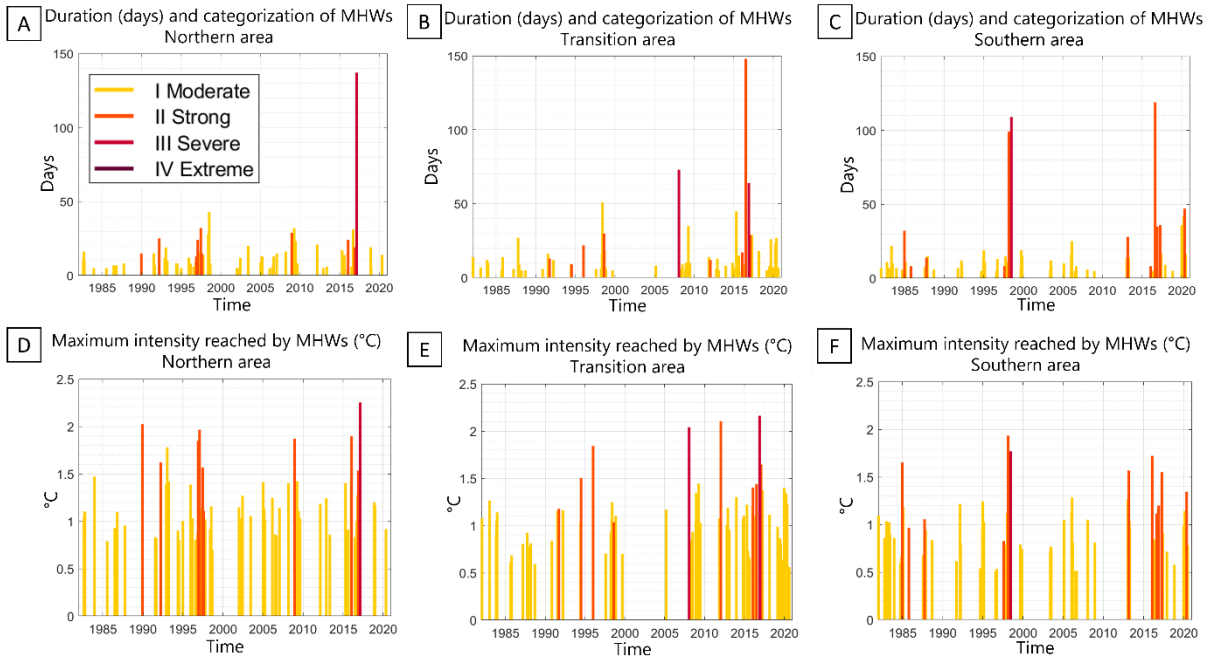

Figure 14: Duration (days, upper row) and maximum intensity (°C, bottom row) for Northern (A, D), Transition (B, E) and Southern (C, F) areas from 1982 to 2020. Every line within the graphs represents a MHW event and colours indicate the categorization of each event (yellow, orange, red and purple for respectively Category I, II, III and IV).

Regarding the intensity over the decades, the mean intensity is always higher for the Northern area than for the two other ones. Conversely, the mean intensity is the lowest for the Southern area (Figure 13C).

For the Northern area, the mean intensity increase has been steady throughout the decades and the strongest event ever recorded was in 2017 with a maximal intensity of 2.3°C (Figure 14D). This MHW had a mean intensity of 1.2°C and was a Category III event. This strong event corresponds to the longest one recorded in this area. Likewise, for the Transition area, a regular increase of the mean intensity is observed with a stabilization for the last decade. The highest intensity recorded was 2.2°C corresponding to a Category II MHW which started in October 2016 (Figure 14E), corresponding to the third longest event (which lasted for 64 days). The mean intensity of this event was 1.3°C. In the Southern area, the strongest event ever recorded was during 1998 while a strong El Niño event occurred with a maximal intensity of 1.9°C (Figure 14F) and a mean intensity of 1.3°C, corresponding to the third longest event (which lasted 99 days). However, it was a Category II event while weaker events were categorized as Category III ones. This is explained by the season during which the MHWs are occurring. Indeed, the strongest event in the Southern area occurred during summer, when the threshold is higher, explaining why it is "only" a Category II event whereas weaker events occurring during winter (with lower threshold) might be categorized as strongest events.

It seems interesting to note that the strongest event recorded was during the last decade for both Northern and Transition areas (Figure 13D). Indeed, 21%, 40% and 38% of the MHW events (respectively for Northern, Transition and Southern areas) that had a maximal intensity superior to 1°C occurred after 2011. In the same way, 36%, 33% and 50% of the events (respectively for the Northern Transition and Southern areas) having a maximal intensity superior to 1.5°C occurred after 2011.

4.4 Case study: the year 2016

4.4.1 2016: an extreme year

Austral autumn, winter and spring 2016 were particularly extreme because of a succession of MHW events throughout the seasons within the 3 areas. The longest MHW recorded was in 2016 in the Transition area and lasted for 148 days (almost 5 months). Only 7 days after this MHW broke, a new one appeared which was the one with the highest intensity recorded for the area (2.2°C). In addition, only 2 Category III MHWs were recorded for this area, and this MHW was one of them. In the same way, the longest event recorded in the

Southern area lasted for 119 days, also occurring in 2016. It corresponded to one of the strongest events of the area with a maximal intensity of 1.1°C. For the Northern area, 7 MHWs were recorded only for the year 2016, being the second most impacted year. Four of those MHWs occurred between September and December 2016 (with durations inferior to 1 month), then followed by the longest event for this area (137 days) corresponding also to the strongest of all areas combined with a maximal intensity of 2.3°C and being in addition the only Category III MHW event of the Northern area.

In 2016, there were respectively 110, 238 and 188 days under MHWs conditions for Northern, Transition and Southern areas. The Transition area was under MHWs conditions during 65% of the year. However, for the Northern area, the year 1997 experienced 136 days under MHWs conditions and 217 days for the Southern area in 1998. Nonetheless, the year 2016 was the only one to cumulate such a long period of MHWs, superior to 100 days, for all 3 areas.

Consequently, as the year 2016 seems to have been anomalously favourable to extreme MHWs events, being the most remarkable year in terms of MHWs duration and intensity, we decided then to focus on that year to understand what may have led to the formation of such consequent events.

4.4.2 Birth, peak and decline of the 2016 marine heatwaves

In the Northern area, 4 relatively short (inferior to one month) MHWs were recorded in spring 2016, from September to December. The first one occurred from early September to early October, the second one from mid-October to early November, the third one from mid-November to early December and the last one occurred in mid-December. All were Category I events except the third one which was a Category II event with a maximum intensity of 1.5°C on November 24th. Then, on January 19th began a Category III MHW which lasted for 137 days with a maximal intensity of 2.3°C on February 28th (Figure 15A).

In the Transition area, 2 major MHWs peaked during late autumn, winter and spring 2016 (Figure 15B). The first one started on May 19th 2016 with a major peak on June 29th and a maximal intensity of 1.4°C. It was a Category II event. Finally, after 148 days of life, the MHW disappeared by mi-October. Then, 7 days later, on October 20th, a new MHW started, with a shorter duration of 64 days. During the first half of November, this MHW almost disappeared but its intensity increased very quickly by mid-November, reaching a maximum of 2.2°C on November 29th. The MHW then disappeared on December 22nd and was a Category

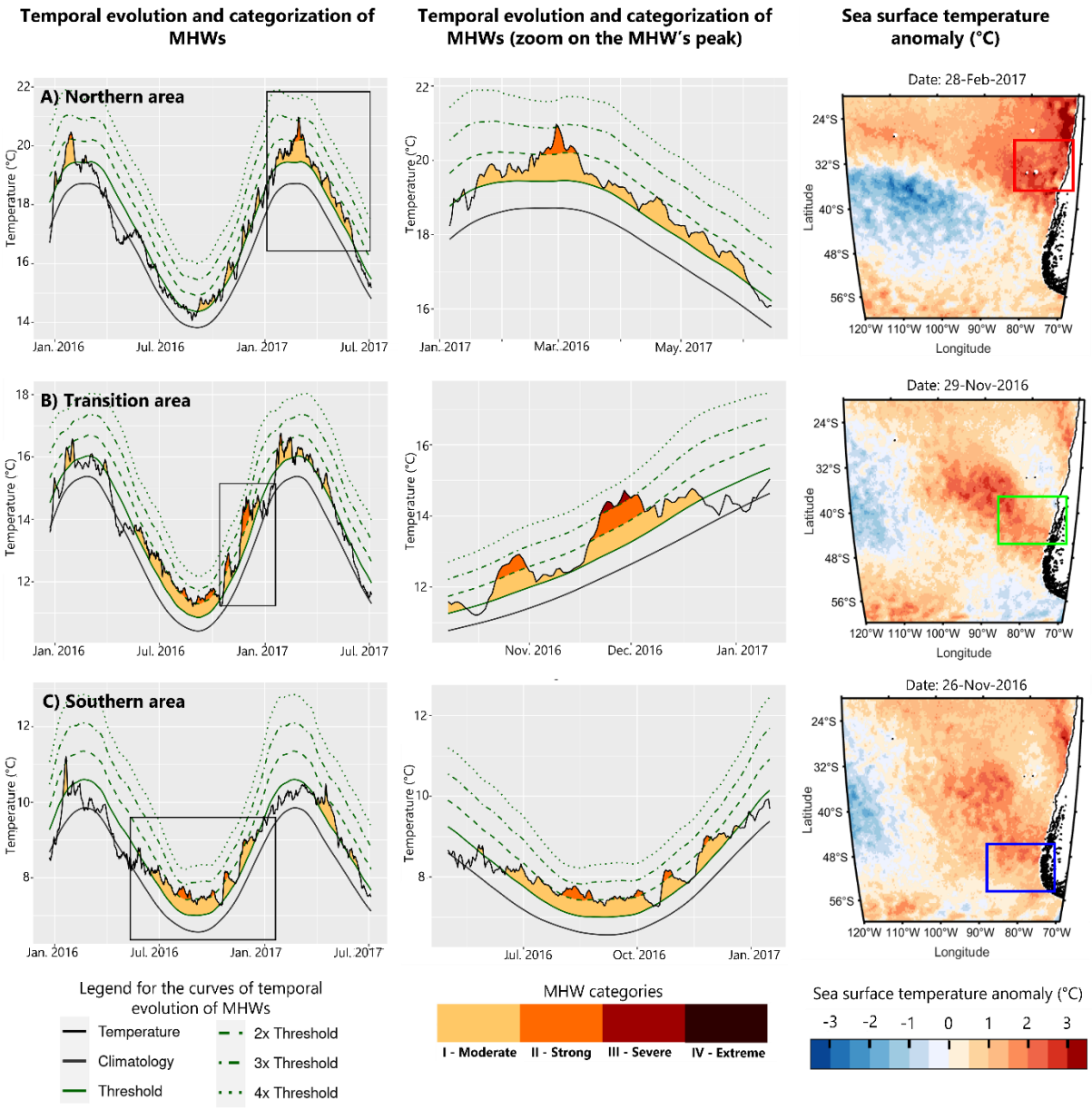

Figure 15: Temporal evolution of the marine heatwaves (MHWs) recorded between January 1st of 2016 and July 1st of 2017 (left column). Those graphs are obtained by averaging the sea surface temperature (SST) over the corresponding area. The central column represents a zoom over the strongest event recorded for each area over this period, highlighted by the black square in the left column. For Northern and Transition area, this event also corresponds to the strongest one ever recorded since 1982. For both left and central columns, the lower line of the graph (black and bold) represents the long-term climatology. The irregular black line represents the daily SST temperature. The green bold line represents the threshold, the first green dashed line is 2 times the threshold, the second green dashed line represents 3 times the threshold and the final green dashed line represents 4 times the threshold. The MHWs categorization is represented by the colours with yellow, orange, red and dark purple corresponding respectively to Category I, II, III and IV. The right column represents the SST anomaly on the day of the main peak of the strongest event. The areas are represented by the coloured squares. Upper line corresponds to Northern area, middle one to Transition area and bottom one to Southern area.

III event. On January 20th 2017, one day after the beginning of the particularly long MHW of the Northern area, a new Category II event began in the Transition area and lasted 31 days, then followed by three shorter Category I events, one starting in February 2017 and the two other ones in March.

In the Southern area, there were 3 successive periods with MHW conditions in winter and spring 2016 (Figure 15C). The first one began on June 17th (about one month after the Transition area experienced MHWs conditions) and peaked on August 18th with a maximal intensity of 1.1°C. MHW conditions lasted for 119 days and dissipated on October 13th. A new MHW started on October 20th with a maximal intensity of 1.7°C and disappeared on November 9th. Nine days later, a new MHW occurred and lasted for 35 days with a maximal intensity of 1.2°C. They all were Category II events.

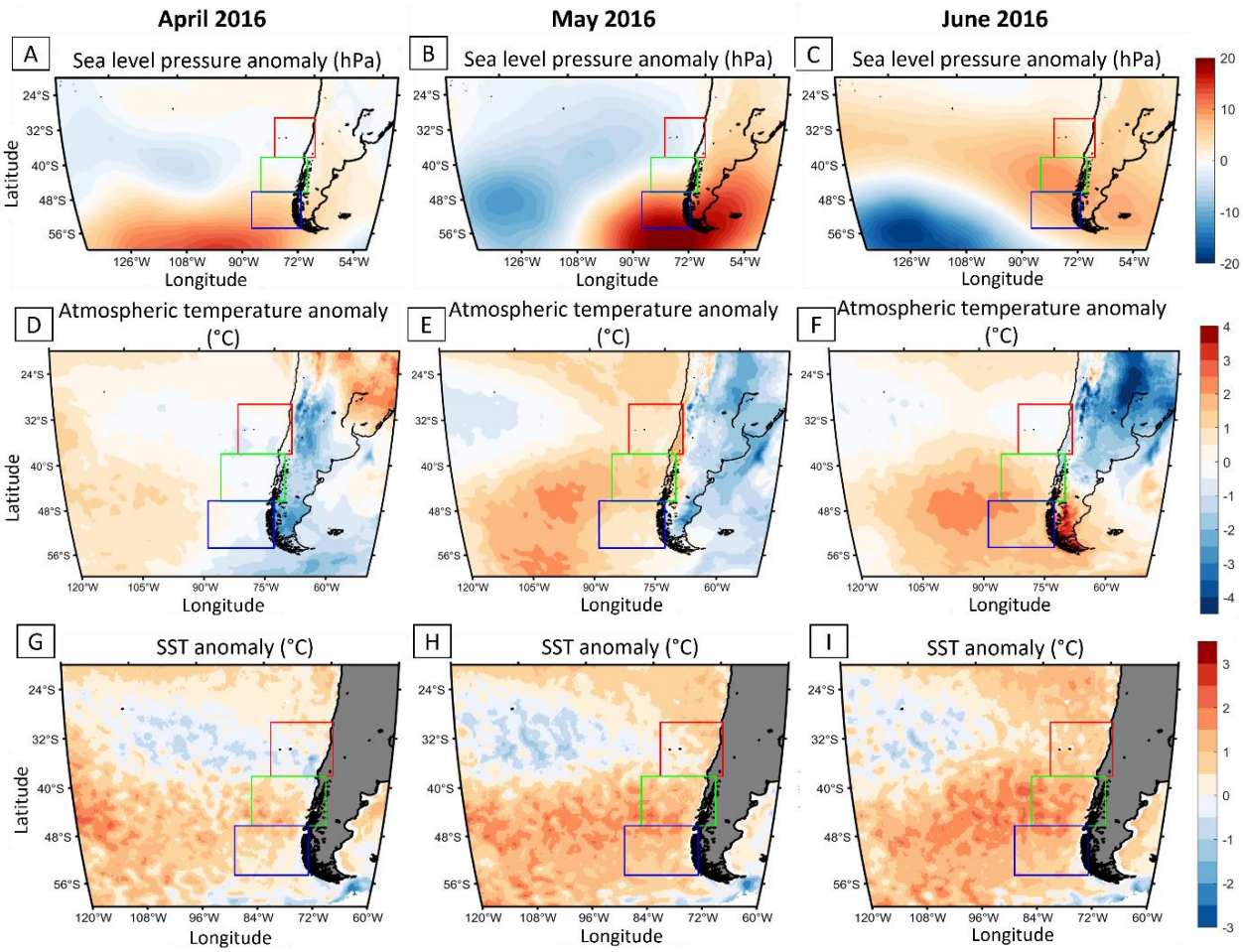

Figure 16: Monthly average sea level atmospheric pressure anomalies (A, B, C), atmospheric temperature anomalies (D, E, F) and sea surface temperature (SST) anomalies (G, H, I), expressed respectively in hPa, °C and °C, for the months of April 2016 (left column), May 2016 (central column) and June 2016 (right column). Colour scale is indicated on the right side of each line. Areas concerned are all located between 20°S and 50°S, and between 50°W and 140°W for pressure anomaly, between 60°W and 120°W for air temperature anomalies and between 60°W and 120°W for SST anomalies.

4.4.3 Atmospheric and oceanic contexts

4.4.3.1 Sea surface temperature

In April 2016, in the tropical Pacific (~5°S to 20°S), positive SST anomalies up to 2.5°C were observable. Those positive anomalies extend along South American coasts, reaching Northern Chile (Figure 16G), with a decreasing gradient towards the South. Between approximately 40°S and 60°S, a large positive anomaly patch was observable between Chilean coasts and 145°W. The warmer part of this patch was between 90°W and 145°W. A core of negative anomalies was observable between the tropical and the mid-latitude warm patches, centred on 100°W and reaching almost only the Northern area's coasts between 33°S and 40°S with anomalies up to -1°C. Nearshore Patagonia, positive anomalies were observable and were the highest off the Transition area's coasts, up to 1.5°C. In May (Figure 16H), the mid-latitude warm patch moved eastward, bringing warm anomalies nearshore. Those anomalies were higher in the Transition area with local anomalies between 2°C and 2.5°C than in the Southern area where anomalies were mostly below 1.5°C. Alongshore, the warm anomalies coming from the tropical Pacific and which have warmed North Chile's coasts merged with the mid-latitude patch, forming a continuous band of positive anomalies along Chilean coasts, the negative anomalies core being more constrained to the open ocean. In June (Figure 16I), warm anomalies were still getting closer to Southern Chile coasts and provoking MHW conditions which started on June 17th in the Southern area. The cold anomalies core was slowly moving away from the coasts. Warm anomalies persisted during winter and early spring, but slowly diminishing. Surprisingly, in early November, a very warm circular patch formed, centred approximately on 90°W and 35°S, West of Juan Fernández Archipelago. At this place, on November 6th, SST anomalies were locally between 1.5°C and 2°C and on November 18th, SST anomalies were locally reaching 4.5°C (Figure 17). The patch then migrated southeastward, losing in intensity, and reached Chilean coasts of the Transition area in late November. The warm patch progressively disappeared in December. It must be noted that for the Transition area, spatially average SST anomalies were always positive during the whole year 2016.

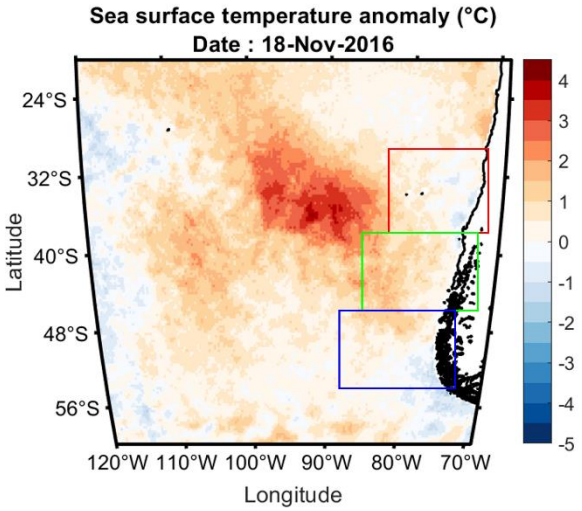

Figure 17: Sea surface temperature anomaly (°C) on November 18th 2016. A paticularly warm patch is observable, centred on 90°W 35°S, with anomalies reaching locally 4.5°C.

4.4.3.2 Atmospheric temperature

In April 2016, monthly averaged air temperature anomalies (with respect to a 39-year climatology) along shore of the 3 areas were close to zero (Figure 16D). However, positive air temperature anomalies were observable far west. In May, those positive anomalies got closer to the coast and positive anomalies were observable offshore and along Chilean coasts (Figure 16E). More precisely, along Chilean coasts of all 3 areas, local air temperature anomalies were between 0.5°C and 1°C, and up to 2°C for the Transition area. Further West, centred on 100°W, a patch with locally 2.5°C anomalies was present. In June (Figure 16F), this patch extended spatially and moved eastward affecting mostly the Southern area but also the Transition area and anomalies up to 4°C were recorded in inland Patagonia. Conversely, in June, the Northern area wasn't touched by air temperature anomalies. In July, the patch's intensity decreased with positive anomalies between 1°C and 1.5°C in the southernmost part of the Transition area and in the northernmost part the Southern area. Elsewhere, anomalies were between 0.5°C and 1°C, but below 0.5°C for the Northern area. The patch then progressively disappeared but positive air temperature anomalies were still observable, on average between 0.5 and 1°C until December 2016. However, in November, a warm anomalies patch was observed West of Juan Fernández Archipelago, centred on 36°S, 95°W. This patch was observable more distinctly than the SST patch, allowing to say that this warm anomaly was already present in October in the tropical Pacific, then moved southeastward and reached the Chilean coast in November. On November 6th and 18th, the core of the warm atmospheric temperature anomaly reached respectively 3°C and 5°C. Contrary to the SST anomaly, the track of the patch hasn't been lost in December and was still present in January and February, affecting only the Northern area's coasts. In January and February 2017, anomalies up to 2°C were present over the Northern area (not shown).

4.4.3.3 Relation between SST anomalies and air temperature anomalies

We spatially averaged SST anomalies and air temperature anomalies over the period 2012-2020 for the 3 areas and performed a cross-validation (Figure 18) to know how they are related. Over the period 2012-2020, air temperature anomalies were preceding SST anomalies with a 10, 1 and 3-days lag respectively for Northern, Transition and Southern areas with a correlation of 0.9291, 0.8748 and 0.8711, respectively. However, having a more specific look to the year 2016 only, air temperature and SST anomalies were occurring with no lag for both Northern and Transition area, whereas for Southern area, SST anomalies were leading air temperature anomalies by 9 days; correlation between the two parameters for all 3 areas being

higher than 0.94 for the year 2016.

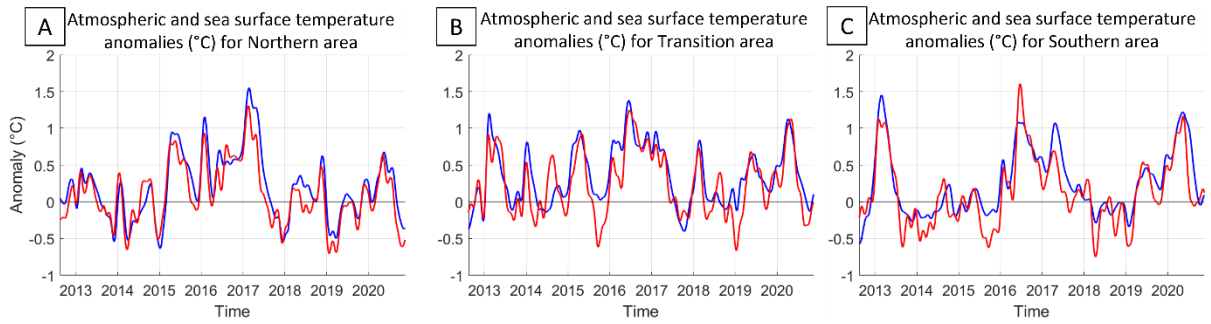

Figure 18: Atmospheric (red) and sea surface temperature (blue) anomalies (°C) spatially averaged over Northern (A), Transition (B) and Southern (C) areas for 2012 to 2020. A 3-month Gaussian filter was applied to the data.

4.4.3.4 High pressure anomalies and winds

During May 2016 (Figure 19B), large-scale positive sea level pressure anomalies were observable South-West of Patagonian tip, with values of about 20 hPa within its core centred approximately on 80°W 60°S, resulting in very stable anticyclonic condition over Southern and Transition areas. The high-pressure system was observable since April over extreme South Pacific Ocean, centred on 100°W with pressure anomaly of 15 hPa within the core, anomalously high pressure reaching Chilean coasts up to 45°S (Figure 19A). Then the high pressure moved northeastward, reaching the highest anomaly values (20 hPa), encompassing the whole Patagonia in May, and then moved northward following the Chilean coast in June with a pressure anomaly of 10 hPa within its core (Figure 19C). Finally, the high-pressure system moved toward eastern Patagonia in July, centred on Falkland Islands with 8 hPa anomalies within the core, and disappeared in August. No remarkable positive or negative pressure anomalies were observed West of Juan Fernández Archipelago in November, where SST anomalies and air temperature anomalies patches were observed.

In order to understand how winds and anticyclonic conditions were related, we studied the wind speed and atmospheric pressure spatially averaged over the 3 different areas. For the Northern area, a wind drop was observable in autumn, beginning in early March and reaching a minimum wind speed of 5.5 m/s in mid-May, and then an increase back until July. Concerning the pressure, no significant diminution or augmentation is observable at the time of the drop in wind speed. In the Transition area, from mid-April to mid-June, wind speed reduced from about 7.6 m/s to 6.2 m/s. Then, the wind speed increased up to 9.1 m/s in early August. In this area (also for the Southern area), pressure and wind speed have opposite patterns, meaning that a high (low) pressure system is associated with reduced (enhanced) winds. Regarding pressure, the increase started from late April until mid-June, reaching 1020 hPa and then started to

decrease until late July. At that time, the correlation between wind speed and pressure is the highest with a 4-day lag, meaning the minimal wind speed was reached 4 days before the highest pressure value. In the Southern area, from mid-March to mid-May, average wind speed decreased from about 10.5 m/s to 7.2 m/s and then increased back until late-June. Concerning the pressure, the opposite pattern is observable with an increase of the atmospheric pressure in mid-March, reaching its higher value of 1018 hPa in mid-May and then decreasing until late-June. In addition, a smaller wind drop is observable at the beginning of August. For this area, the correlation is highest when wind speed precedes the pressure by 3 days.

For both Transition and Southern areas, the drop in wind speed was associated to a drop in the u-component (eastward component). For the Southern area, the u-component of the wind speed was almost zero in early May. For the Transition area, the u-component of the wind speed is fully eastward over the 2012-2020 period except in mid-May 2016, having a very low wind speed with a westward component. In early August 2016, a wind drop in both u and v-components (more important for the u-component) is observable for the Southern area. In all 3 areas, the wind speed drop corresponded to the lowest value over the period 2012 to 2020 and for the Southern area only, the high-pressure peak corresponded to the highest recorded over the same period.

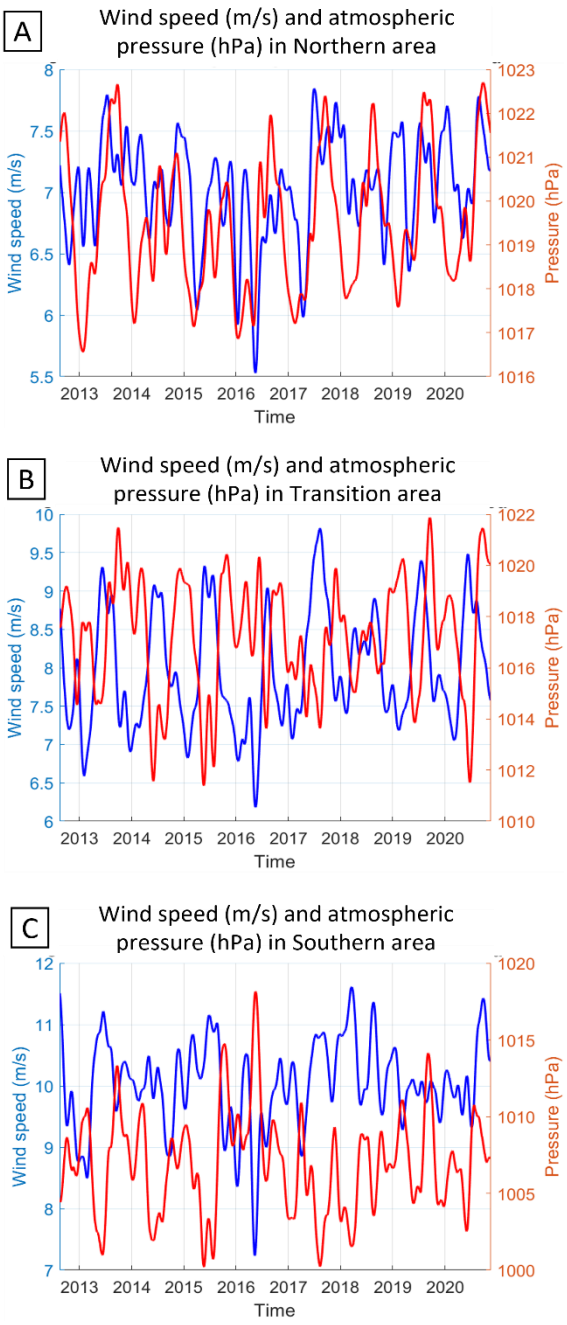

Figure 19: Wind speed (blue) and sea level atmospheric pressure (red) from 2012 to 2020 for Northern (A), Transition (B) and Southern (C) areas. A 3-month Gaussian filter was applied to the data. For a better visualisation of the variations, y-axis' scales differs.

4.4.3.5 Heat fluxes

According to the timeseries of the heat fluxes for the 3 areas, during autumn and winter 2016, the heat transfer from the ocean to the atmosphere was lower than during the other years

(2012-2020) in both Transition and Southern area. This reduction of the heat transfer is particularly important for the Southern area. The comparison between monthly total net heat fluxes (Qi) for 2016 and monthly Qi values averaged over the period 2012 to 2020 was realised. In April 2016, the heat transfer from the ocean to the air was higher than the average by 7, 20 and 32 W/m² for respectively Northern, Transition and Southern areas. In May 2016, the heat transfer was lower than the average by 33, 38 and 39 W/m², being the strongest anomalies for the Northern and Transition areas. In June 2016, the heat transfer was close to the average for the Northern area and 26 W/m² below average for the Transition area. For the Southern area, the strongest anomaly was reached in June with values of 52.82 W/m² below average. This reduction of the heat transfer from the ocean to the atmosphere was induced by lower latent heat transfer. When looking at the spatial distribution of the heat transfer (Figure 20), in April 2016 a large patch of negative anomalies (i.e. the heat transfer was reduced) centred on 105°W and extending up to 85°W is present (Figure 20A). In May, this patch intensified and moved eastward up to Patagonian coasts. A remarkable wide band of highly negative anomalies along Chilean coasts extend to approximately 100°W, with values up to -70 W/m² in the 3 areas of interest (Figure 20B). A large positive anomaly core is observable from 100°W to further West (meaning that the heat loss was higher than usual). In June, low positive anomalies are present in the Northern area, but along the Transition area and particularly the Southern area, heat loss anomalies were especially low, up to -100 W/m² (Figure 20C). Then the anomalies are becoming weaker, except for November: a large negative anomaly patch is observable where the warm SST anomalies and air temperature anomalies were observable at the same period.

In addition, albedo was also lower than usual during spring and winter 2016 for both

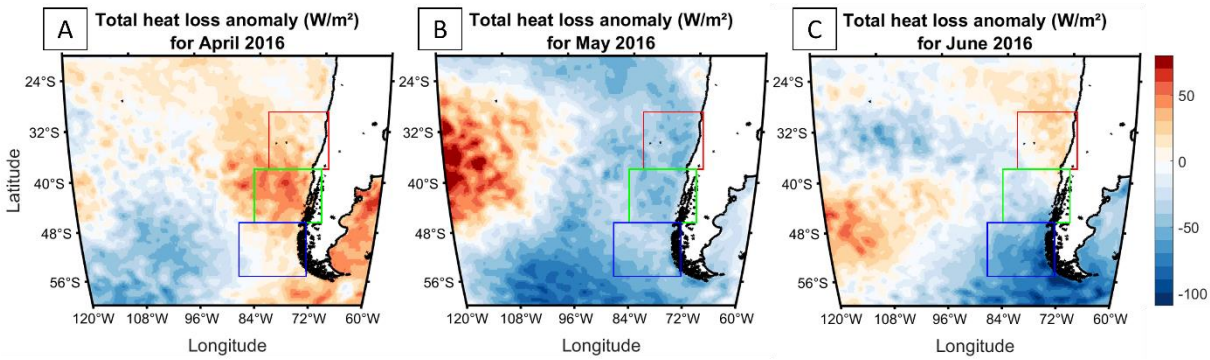

Figure 20: Monthly anomaly of total heat transfer (in W/m²) from the ocean to the atmosphere. Total heat transfer (Qbec) corresponds to the sum of the thermic radiation, (Qb) latent heat (Qe), and sensible heat (Qc) fluxes. The anomaly has been calculated according to the 2012 to 2020 average. Positive (negative) anomaly indicates a higher (lower) than usual heat transfer from the ocean to atmosphere. For example, if anomalies are corresponding to -100 W/m², it means than the heat transfer was reduced by 100 W/m² compared to the 2012-2020 average.

Transition and Southern area (not shown). The total cloud coverage was not significantly lower than usual during winter 2016 for all 3 areas, contrary to the lower cloud coverage which was the lowest ever reached over the 2012-2020 period in the Northern and Transition areas, respectively in mid-May and late July 2016 (not shown). For the Southern area, low-cloud coverage started to decrease in mid-May and reached a minimal value in late August, not being the lowest coverage reached between 2012 and 2020 but the second one.

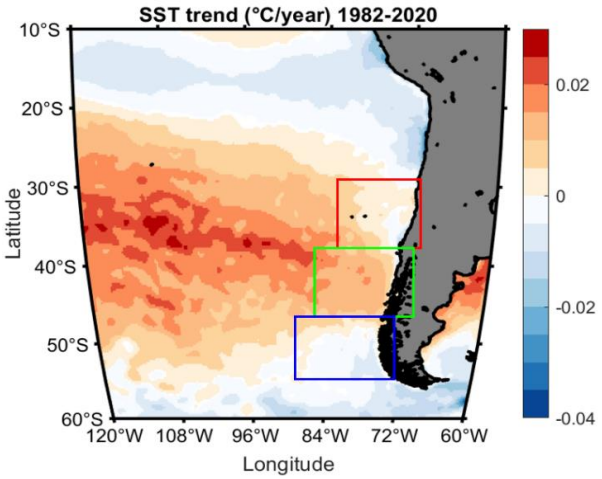

Figure 21: Significative (according to p-value<0.05) sea surface temperature (SST) trends (°C/year) over Southeast Pacific Ocean from 1982 to 2020. Areas where no significative trends were observed are shown in white.

4.5 Long-term trends for SST and MHWs

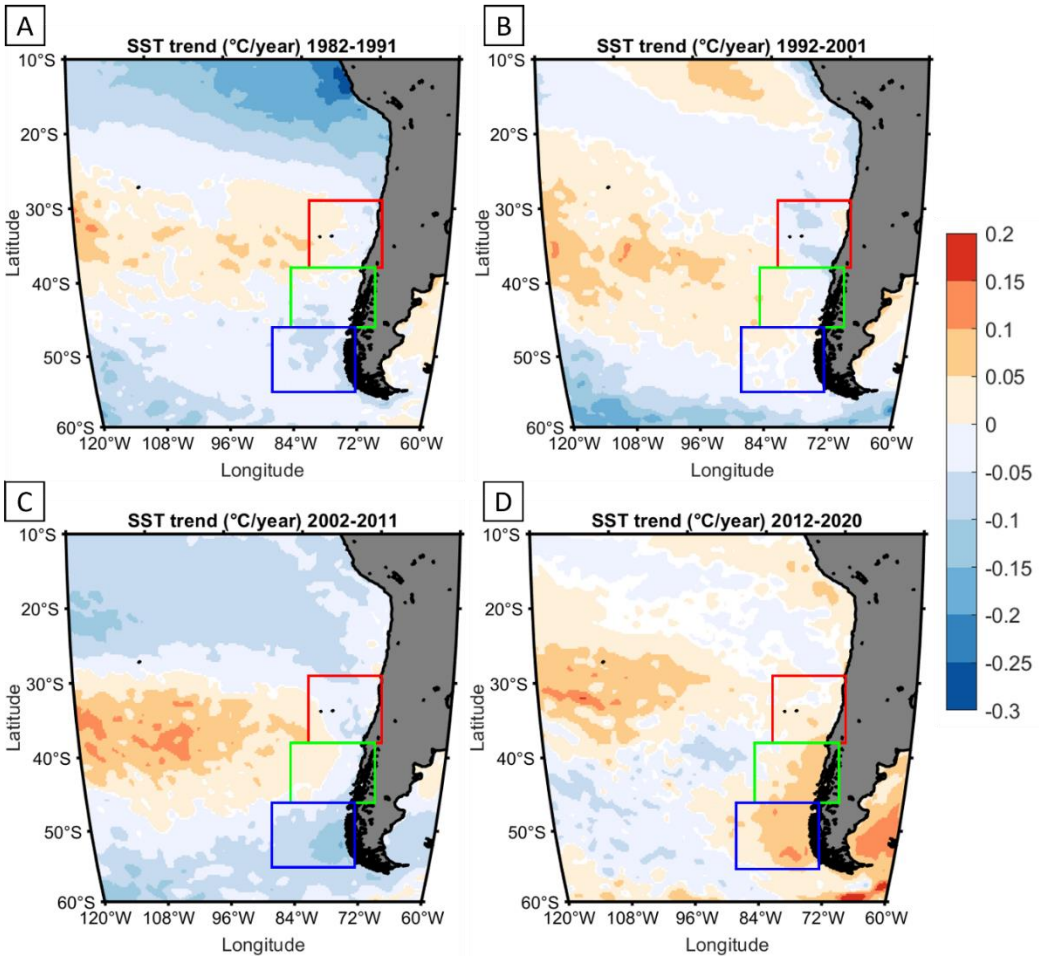

Figure 22: Significative sea surface temperature (SST) decadal trends (according to p-value<0.05) in °C per year for (A) 1982-1991, (B) 1992-2001, (C) 2002-2011 and (D) 2012-2020. Areas where no significative trends were observed are shown in white.

SST trends from 1982 to 2020 show that the Central South Pacific has been particularly hit by warming during the last 40 years (Figure 21). A very large patch from the Tropics to mid-latitudes suffered from positive trends, about 0.03°C per year within the patch's centre. The patch reaches South American coasts from 30°S to 47°S, except at 37°S where a cold trend is present. The coasts between 38°S and 47°S, are hit with trends ranging from 0.005 to 0.015°C per year. The Transition area is the South American coast portion facing the highest warming trends.

When looking at the decadal trends (Figure 22), we can see that during the three first decades, Chilean coasts did not suffer from warming trends (Figures 22A, 22B, 22C). On the contrary, cooling trends are observed. However, during the last decade (2012-2020), all Chilean coasts are affected by the warming, especially the Western Patagonia (but also Eastern) with warming trends of +0.05°C to +0.1°C per year (Figure 22D). Note that the Central South Pacific has also been badly hit during all 4 decades.

HeatwaveR algorithms can also provide the MHWs trends (Figure 23). Thus, we performed the analysis over a reduced portion of the Southeast Pacific Ocean from 1982 to 2020, focusing only on our 3 areas of interest. The results are the trends of frequency of MHWs within each pixel. Consequently, an increase of the number of MHWs is remarkable at mid-latitudes especially at lower latitudes than 45°S. Along Transition area coasts, a positive trend is also present but not significant. Moreover, a negative trend is observable at 37°S.

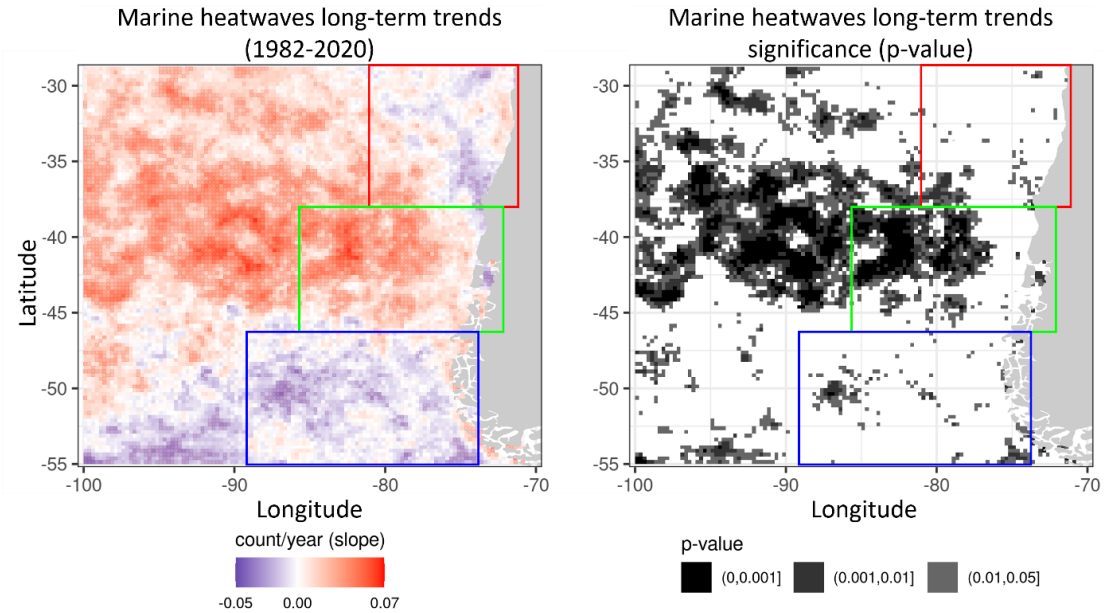

Figure 23: Marine heatwaves (MHWs) trends (left) and significance of the trends according to the p-value (right). The trend is calculated according to the number of MHWs that have occurred in each pixel from 1982 to 2020. Consequently, a positive (negative) trend significate that the number of MHWs is increasing (decreasing) with time.

5 DISCUSSION

5.1 Choice of marine heatwave detection parameters

Our detection of MHWs follows the criteria given by Hobday et al. (2016), with a climatology based on almost 40 years of SST satellite data (1982-2020) and a threshold defined as the 90th percentile. However, MHWs' definition (and consequently their detection) is very subjective as the length of the climatology and the threshold chosen will define the number of events, their duration and their intensity.

The definition of the climatology is primordial as it is used to define the MHWs occurrence and metrics associated. A fixed baseline climatology (used in this study) allows to consider the total SST variability including the long-term mean warming, and not only the variability around the mean, considering the global warming and allowing for example to assess the response of the marine organisms to this warming. Indeed, oceans' mean temperature are rising due to global warming, but the variability around the mean remains steady *(Jacox, 2019)*, thus over long-term periods, MHWs are more likely driven by the mean SST than by the SST variance *(Oliver et al., 2019)*. In addition, the species have evolved in response to what we call "normal" conditions but will in the future (and are already) experiencing rapid warming tendencies, possibly exceeding their thermal tolerance before they will be able to adapt *(Jacox et al., 2020)*. Hence, taking into account global warming is necessary. However, this kind of climatology might be obsolete in future works, as "normal" conditions might be always above the threshold; consequently, the definition of MHWs as "discrete events" will not be respected anymore. Therefore, the length of the timeseries used to build the climatology is also very important. What if the climatology is based on a 1980-2010 period or on a 1980-2020 period? Will the MHWs calculation be similar? Not considering the last decade would imply the omission of the warming trends and MHWs detection would be modified. For our study case, during our testing phases, we tried to detect MHWs from 1982 to 2020 but with a 30-year based climatology (1982-2011). As the last decade's warming was not considered, the number of MHWs detected was almost multiplied by two, and the event's intensity was higher, particularly for the last decade. Different studies are using a 30-year baseline climatology which stops at the beginning of the 2010s *(e.g. Jacox et al., 2020; Sen Gupta et al., 2020; Carvalho et al., 2021)*, but other authors are using the whole data available, meaning a longer than 30-year baseline, which stops at the year (or a few years before) of the papers publication *(e.g. Scannell et al., 2016; Benthuysen et al., 2018; Manta et al., 2018; Omneya et al., 2021)*. To solve the

problem, a solution could be the use of a moving climatology which would allow to not consider the extreme conditions. However, for now, the length of the dataset available might not be long enough to consider a moving climatology but could be in future works.

On top of that, the choice of the threshold varies according to authors which also modifies the MHWs detection. Two kinds of thresholds are used: moving ones, calculated according to the climatology thus allowing to detect MHWs for each year and each season, and fixed thresholds based on a fixed SST value chosen by the author. Fixed thresholds are generally used to know if one particular species will be affected by SST exceeding its thermal tolerance during MHWs. However, moving thresholds are the most used, particularly the 90^{th} percentile *(e.g. Oliver et al., 2018; Sen Gupta et al., 2020; Mawren et al., 2021)* as it allows to detect all MHW events that may affect the ecosystems and not only the strongest ones. This threshold has the same advantage and inconvenient: it is relatively easy to exceed it, allowing to detect lots of events, even the minor ones. In our study, we used this threshold as it allows us to do a global assessment of the MHWs that have occurred offshore Central and Southern Chile. However, other authors are using higher percentiles to avoid smaller events or to determine more easily when the strongest events occurred. Holbrook et al. (2019) for example are using 98^{th} percentile, Darmaraki et al. (2019) are using the 99^{th} percentile and Frölicher et al., (2018) are even using the 99.99^{th} percentile to detect only the most extreme events.

Some authors use monthly average SST data to calculate MHWs (including for climatology and threshold calculation) instead of daily SST data *(e.g. Scannell et al., 2016; Jacox et al., 2020)*. Jacox et al. (2020) justify it by saying that the definition of MHWs of at least 5 consecutive days of warm anomalies does not consider the thermic retention of the oceans, whereas one month would be more suitable. Moreover, MHWs damages on ecosystems has been attributed in most of the case to longer than one month events (e.g. species migration will not be done within 5 days). In addition, the authors precise that if the definition allows MHWs to be detected several times a year at the same place, MHWs cannot be considered anymore as occasional events but maybe as the becoming normal conditions of that place. Thus, considering monthly SST would be more accurate to detect only the significant MHWs that may have an impact on ecosystems.

For now, there is no optimal solution to define MHWs. None can take into consideration all parameters impacting the species and the ecosystems. In their definition of MHWs, Hobday et al., (2016) even specify that "the metrics can, of course, be modified to suit the specific application". Therefore, all the definitions might be correct, depending on what we are looking

for. However, this could pose a problem for the studies inter-comparison: if different threshold or baseline climatology are used, the description of a single event might differ according to the authors.

5.2 General context

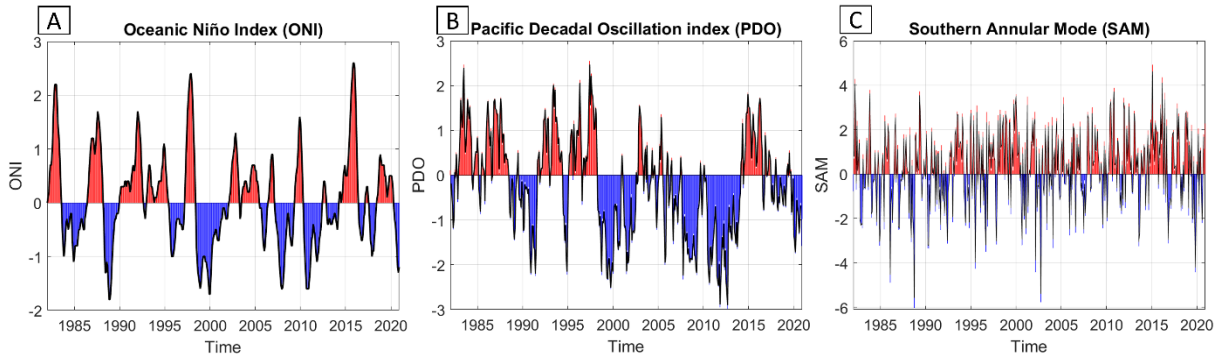

Figure 24: Different remotes forcings expressed by their index. (A) Oceanic Niño Index for ENSO monitoring (ONI), (B) Pacific Decadal Oscillation (PDO) index, (C) Southern Annular Mode (SAM) index. Red indicates a positive period and blue a negative period. PDO and SAM index are expressed with a 3-month Gauss filter, represented by the black bold line. ONI calculation is already based on a 3-month average. The scale differs according to the index.

During the first half of 2016, Patagonia was experiencing very uncommon conditions with the presence of a severe drought which has reduced the streamflow by -30% to -60% *(Garreaud, 2018)*, in a global context of drought in subtropical Southeast Pacific Ocean since 2010 *(Garreaud et al., 2020)*. That context was partly due to large-scale climatic forcings. Indeed, from the mid-2000s and until mid-2014, cold phase of the PDO was predominant and then switched to a warm phase until mid-2017 (Figure 24B). In addition, from 2011 to 2013, the ENSO cold phase was dominant and switched to warm conditions in 2014 until mid-2016 (Figure 24A), being one of the three strongest El Niño events ever recorded with the 1982-1983 and 1997-1998 ones. Because of its importance, it has been popularly named "Godzilla El Niño". Garreaud (2018) has shown that this El Niño event was associated during 2015 with strong positive sea level atmospheric pressure anomalies (>7 hPa) at extratropical latitudes. However, during austral autumn (March-April-May), we found that those atmospheric pressure anomalies were much higher (Figure 25), with seasonal average up to 10 hPa. We did not perform a comparison between 2016 wind speed and long-term wind speed, but Garreaud (2018) did it specifically off Chiloe Island (42.5°S, 74.3°W, corresponding to our Transition area) and shown reduced winds from late-May to mid-June (about twice inferior to the long-term average), coherent with what we found in part 4.4.3.4. This reduced wind pattern is consistent with the presence of the large anticyclonic system West of Southern Patagonia and was associated with the Godzilla El Niño event. Indeed, when a positive El Niño phase

occurred, there are increases in the occurrence of blocking anti-cyclones West of Antarctic Peninsula *(Rutllant & Fuenzalida, 1991)*. Moreover, a very strong positive SAM event also occurred at the same period, from early 2014 to late 2016 (Figure 24C). In summer 2016, because of the presence of a very strong dipole between high and mid-latitudes, SAM values were very high. It should be noted that SAM trends are becoming more and more positive over the last decades *(Fogt & Marshall, 2020)*, partly due to ozone depletion and greenhouse gases which exacerbate SAM phenomenon *(Gillett & Thompson, 2003)*. Nonetheless, usually ENSO and SAM have negative correlation (*Gong et al., 2010*; see part 1.1.2.3), thus the synchronisation of very strong positive events of both phenomena seems confusing. However, as the two phenomena have the same consequences over Chilean Patagonia, meaning high pressure systems South of Patagonia, reduced Westerly winds at mid-latitude and higher temperatures, their combined effects might exacerbate their consequences. And effectively, the drop in wind speed we observed in late autumn 2016 and the high pressure associated were the highest ever recorded at least over the period 2012-2020.

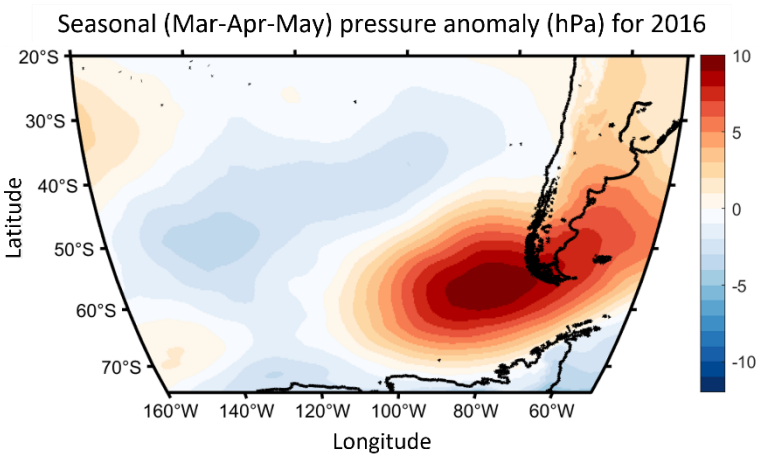

Figure 25 : Seasonal pressure anomaly (hPa) averaged on March-April-May 2016.

SAM as a potential maintainer or activator of MHWs has been poorly studied, although it may lead to the typical atmospheric processes which may lead in return to MHWs formation, such as persisting high-pressure systems and reduced winds. However, it has been cited by Su et al. (2021) as a factor maintaining the MHWs in combination with ENSO on Kerguelen Plateau (extreme South Indian Ocean) and by Salinger et al. (2019) and Perkins-Kirkpatrick et al. (2019) as a factor having led to anomalously high pressure system and reduced Westerly Winds (same processes as for our case study) around New-Zealand, conducing to MHW formation in 2017-2018.

Additionally, we did not focus on the years 1997-1998, but the MHWs detection has shown large events especially for the Southern and Northern areas during these years. Simply, note that those extreme events were also linked to strong positive phases of both ENSO and SAM (Figure 24).

5.3 Marine heatwaves in 2016

5.3.1 Formation and processes

In early and mid-March 2016, the wind speed started to decrease in Northern and Southern areas respectively. In mid-March also started a rise of the atmospheric pressure and of the SST anomalies in the Southern area.

In April 2016, the low-cloud coverage was reduced in both Northern and Transition areas. The air temperature anomalies were almost zero alongshore of the 3 areas. However, SST anomalies were already positive since the beginning of the year 2016, but were not high enough to trigger a MHW, as during summer the threshold above which MHWs are detected is higher. In mid-April, the atmospheric temperature anomalies started to increase in the Transition and Southern areas. In the Transition area only, the wind speed started to decrease, associated with a pressure increase in late April. As well, the SST anomaly coming from the extratropical Pacific (~55°S, 130°W) started to increase in the Transition area in mid-April. Within the 3 areas, in April, the heat transfer ocean-atmosphere was higher than the 2012-2020 average.

In May 2016, positive SST anomalies coming from the extratropical South Pacific got closer to the coasts, bringing anomalies which were higher for the Transition area than for the Southern area. Low-cloud coverage started to decrease in the Southern area. In mid-May, atmospheric temperature reached its highest values in the Northern area. At the same time, the wind speed reached its lowest value over the 2012-2020 period for both Northern and Southern areas, and the Transition area experienced unusual weak westward winds. It was the unique time interval during which westward winds were dominant in the Transition area over the 2012-2020 period. At the same time, the highest pressure peak was recorded for the Southern area. In May 2016, for all 3 areas, the heat transfer from the ocean to the atmosphere was lower than average. This deficit of heat loss was the highest observed for both Northern and Transition areas. Indeed, with the lowest wind-speed ever recorded for both Northern and Southern area and high-pressure systems over Transition and Southern area, conditions were favourable to low sea-air fluxes. On May 19th, the Transition area started to experience MHWs condition due to the combination advection of warm SST anomalies, high pressure system and weaker winds associated to warm atmospheric temperature anomalies and heat loss reduction. Those MHW conditions lasted for 148 days in that area (almost 5 months).

In mid-June, the pressure and the wind speed were respectively the highest and the lowest ever recorded for the Transition area, though Strub et al. (2019) indicates that in the

Transition area, poleward winds have the strongest speed at that period. Those conditions have induced a reduction of the ocean's heat transfer. In addition, the SST anomalies, still coming from the extratropical Central South Pacific, reached its maximum in mid-June in the Transition area, and were high enough to trigger a MHW in the Southern area on June 17th (which lasted for 119 days) and to make peak the MHW in the Transition area on June 29th, favourited by the co-occurrence of maximal pressure, very low wind speed, high air temperature anomalies, which resulted in a low heat transfer from the ocean to the atmosphere.

In early October, wind speed reached high values during a few days in both Transition and Southern areas (associated with low pressure), coincident with the dissipation of the MHW on October 13th for both areas. In early October, advection of warm waters coming from extratropical South Pacific triggered new MHWs in all 3 areas in mid-October (October 20th for both Transition and Southern area and on October 21st for Northern area). In early November, the warm-water anomalies decreased, leading to a break within the MHW period in Northern and Southern areas and the MHW in the Transition area almost disappeared. Meanwhile, a warm SST patch formed very quickly West of Juan Fernández Islands in early November 2016, with an SST anomaly increase of 2.5°C in only 12 days, from 6th to 18th of November. Same for atmospheric temperatures with a rise of 2°C over the same period. Both atmospheric and oceanic warm patches moved southeastward and reached the coasts in late November, encompassing the three areas and coinciding with the new apparition of MHWs in Northern and Southern area (both on November 18th) and to the strengthening of the MHW in the Transition area. The MHW peaked in the Southern area on November 26th, then the anomalies started decreasing. In the Transition area, the anomalies were getting closer to the coast until November 29th, coinciding the MHW peak in that area. In the Northern area, the MHW was not that strong because of the presence of a coastal negative anomaly signal at approximately 37°S, corresponding to Punta Lavapie, an area where upwelling favourable winds are predominant from September to February *(Letelier et al., 2009)*, explaining the negative trends of SST anomalies often observed in this area. However, the warm patches moved northeastward in mid-December and the anomalies were decreasing. Nevertheless, in late January 2017, both SST and atmospheric temperature anomalies patch increased back, provoking the 137 days (4 and a half months) MHW in the Northern area (which was, by the way, the strongest event ever recorded along Chile).

It is important to note that for the Southern area, SST anomalies were occurring days before air temperature anomalies and for Transition and Northern areas, the anomalies were

occurring with no lag. In addition, in our 3 study zones, the SST is almost always higher than the air temperature (Figure 10). This would signify that the autumn-winter-spring MHWs in 2016 were led by oceanic processes (warm water advection in that case coming from extratropical South Pacific) and maintained by atmospheric condition (high-pressure system associated to lower winds, unusual warm air temperature and thus reduce heat loss from the ocean), preventing waters to cool during winter.

5.3.2 The warm patches

The warm patch we described in the extratropical South Pacific at mid-latitude (see part 5.3.1), bringing positive SST anomalies to Patagonia through the Pacific Gyre, has been described in different studies and is part of the South Pacific Ocean Dipole (SPOD). The dipole is composed of an extratropical positive SST anomalies patch (corresponding to the one we highlighted) centred on about 58°S, 125°W and a subtropical negative SST anomalies patch centred on the eastern coast of New-Zealand *(Saurral et al., 2020)*. The spatial distribution of this dipole experiences low variability but its amplitude varies according to seasons *(Guan et al., 2014)* and to large-scale forcing (e.g. ENSO, PDO; *Chatterjee et al., 2017; Saurral et al., 2020*). The main variability of the dipole is explained by ENSO *(Li et al., 2012; Chatterjee et al., 2017)*: when positive phases of ENSO are occurring, the warm anomalies are enhanced in the extratropical dipole. As a strong El Niño event was present in summer 2015-2016, warm anomalies of the extratropical dipole were able to strengthen, provoking the MHWs we described. In addition, dipole's SST anomalies are subject to eastward propagation *(Li et al., 2012)* explaining why they reached Patagonia and provoked the MHWs.

The warm patch we described West of Juan Fernández Archipelago that formed in November 2016 and strengthened in January 2017 was probably linked to a "coastal El Niño" *(Garreaud, 2018; Rodríguez-Morata et al., 2019)*, whose characteristics were a strong and rapid warming of the easternmost Equatorial Pacific in January 2017 followed by other warm pulses in February and March, associated with very weak Tradewinds from January to April 2017. In fact, the whole Central Pacific experienced a very strong El Niño in 2015-2016, but the easternmost Central Pacific experienced a "longer" El Niño in summer 2017 *(Garreaud, 2018)*. In its study, Garreaud (2018) highlights a tongue-shaped warm SST coming from Equatorial Pacific and extending southeastward to the coasts of our Northern area, in accordance with what we described in part 5.3.1. This warm patch resulted in the formation of the most intense MHW in the Northern area, which lasted from January 19th to June 4th 2017.

5.4 SST and marine heatwaves trends

We found that the Transition area is particularly impacted by positively increasing MHWs metrics. Indeed, although MHWs metrics have globally increased over the decades within all 3 studied areas, the increase is particularly important for the Transition one. It is the only area in which all metrics, except the number of events, have constantly increased over the decades. Concerning the number of events, an exceptional increase is observed over the 2012-2020 period (only 9 years), totalling 45% of all the events that have peaked in this area. In addition, regarding the long-term MHWs trends (1982 to 2020), the Transition area is the only one to be impacted by the positively increasing trends (Figure 23). Those MHWs trends showed a tongue-shaped positive patch where the number of MHWs detected along the years have increased, coming from the Central Pacific and reaching Chilean Coasts in the Transition area.

Regarding the decadal SST trends, during the three first decades, a positive trend, tongue-shaped, is observable and centred approximately on 35°S. Cooling trends are always observed nearshore of South America. Nevertheless, the last decade shows a totally different pattern, with positive anomalies everywhere (except a horseshoe pattern of negative trends), particularly high along Patagonian coasts with +0.05°C to +0.1°C. According to the long-term SST trends (1982-1980), not only the Transition area is fully impacted, but it is also the only South American Pacific coast (South of 10°S) impacted by positive trends. We showed that the SST warming reached 0.005 to 0.01°C per year along the Transition area shores. SST trends are coherent with what was observed by Roemmich et al. (2016): a tongue-shaped warm patch, with a warm core between 30°S and 40°S and coming close to the coast between 38°S and 47°S. However, in their study, Roemmich et al. (2016) observed a cooling trend along Chilean coasts, contrary to what we found. The difference might be linked to the different time series used: their study has been realised from 1981 to 2015, whereas in our study we also encompassed the end of the last decade. Yet, we showed that the last decade is particularly important in terms of warming, probably explaining the difference between the two studies. In addition, they performed their study within the whole subtropical Pacific, allowing to highlight that the warming in the South Pacific is the highest at 33°S, 158°W, depicting that Patagonia is influenced by the Central South Pacific. Note that Gutiérrez et al. (2018) found that winter SST has increased from 2010 to 2016 in Northern Patagonian fjords, being maximal in 2016, the winter we observe the very long MHW in both Transition and Southern areas.

In addition, we noticed that MHWs trends and SST positive trends from 1982 to 2020 share the same distribution pattern. It is explained by the fact that MHWs are highly related to

increasing SST across the globe *(Frölicher et al., 2018)*.

5.5 Marine heatwaves consequences on fjords ecosystems

MHWs' impacts on species depends on MHW's intensity, duration but also vertical extent. Few studies have been realised on what consequences could have MHWs on fjord environments and none on Patagonian fjords. However, we suggest that major consequences occurring in other oceans or seas might be applicable to our studied areas, such as species communities shifts or mass mortality. For example, a shift from mostly autotroph (algae) dominated to heterotroph (invertebrate) dominated was observed in intertidal environments of Gulf of Alaska (including fjords) after a MHW which lasted from 2014 to 2017 *(Weitzman et al., 2021)*. Weitzman et al. (2021) reported that this community shift resorbed 5 years after the resilience of the MHW. In Chilean Patagonia, decrease in microbial richness has already been observed associated with seasonal increase of sea temperatures, particularly in winter *(Gutiérrez et al., 2018)*. This would probably be exacerbated as MHWs are projected to be more numerous, as we saw in part 4.5.

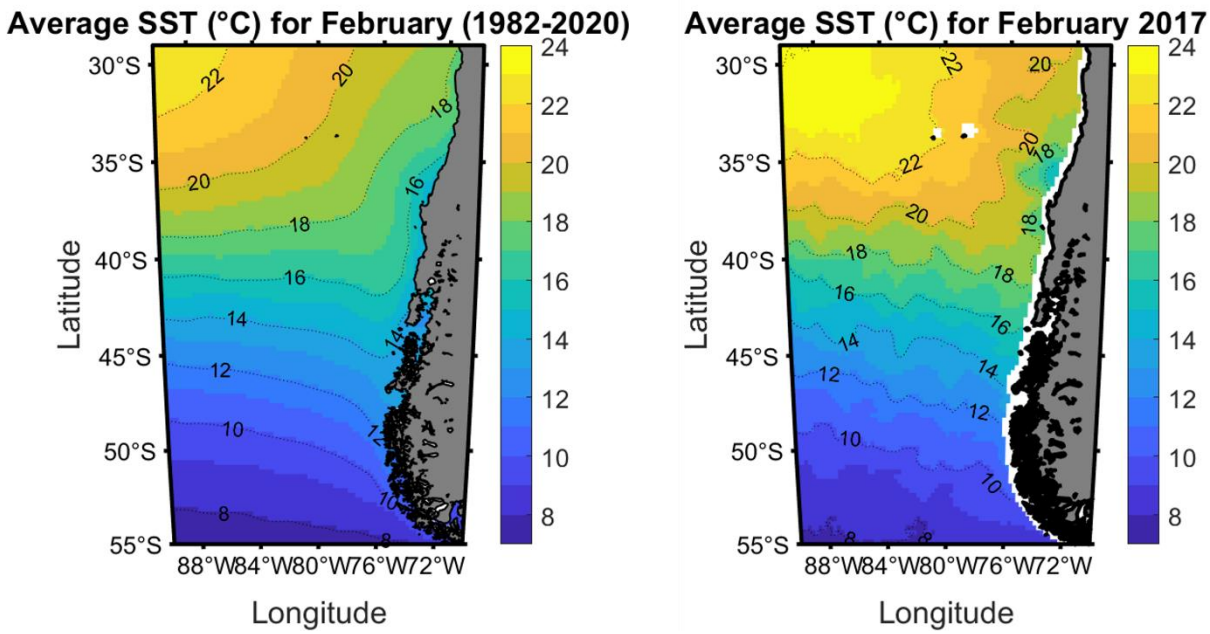

Figure 26: Sea surface temperature (°C) long-term monthly averaged over 1982 to 2020 period for February (A) and monthly average for February 2017 (B).

Nearshore Northern Patagonia (41°S-45°S), long-term average SST in February is between 14°C and 15°C (Figure 26A). However, in February 2017, the strongest ever MHW event was recorded. Consequently, in February 2017, the SST was higher than average, near 17°C in Northernmost Patagonia. Optimal temperature for Atlantic salmon (*Salmo salar*) growth is between 12°C and 18°C *(Elliott & Elliott, 2010)*, beyond 18°C, salmons' growth performances are reduced *(Hevrøy et al., 2012)*. In any event, cold waters of Northern Patagonia

are supposed to be optimal for salmon's growth, even during summer months (Figure 26A). Nevertheless, during the summer 2017, the SST nearshore was nearly 2°C higher than average (Figure 26B), becoming close to the upper limit of optimal temperature growth for Atlantic salmons. Consequently, a such increase of the SST during summer MHWs could provoke a thermal stress for salmons and alter their growth performances, having in return economic repercussions as it has already been observed in the past, for instance during the 2015-2016 Tasmanian MHW *(Oliver et al., 2017)*.

It seems important to note that a HAB occurred in austral summer 2016, from February to May *(León-Muñoz et al., 2018; Armijo et al., 2020)*, in Northern Patagonian inner seas and along Pacific coasts of Chiloe Island (41°4'S to 43°2'S, corresponding to our Transition area) enhanced by the reduced freshwater riverine inputs, higher temperatures and increased solar radiation *(Garreaud, 2018)*. This HAB was the worst ever recorded for Patagonia, causing massive mortality in aquaculture farms with economic losses of several hundred million dollars *(e.g. Díaz et al., 2019)*. HAB were often described as one of the consequences of MHWs *(e.g. NOAA Climate, 2015; Roberts et al., 2019)*, but this HAB occurred before the MHW we detected in the Transition area (starting on May 19th 2016). However, the spatial resolution of the SST data we used to perform our MHWs detection is too coarse to detect the MHWs within the inner seas, preventing us to know if they experienced more numerous or longer MHWs than the open ocean did and if the HAB coincided with a MHW event.

Chilean Patagonian fjords are experiencing hypoxic conditions due to fjord alimentation by low-oxygen Equatorial waters filling the deep micro-basins *(Silva & Vargas, 2014; Pérez-Santos et al., 2018)*, a strong stratification which provide deep waters to be re-oxygenated by vertical mixing *(Silva & Vargas, 2014)* and anthropogenic activities (sewage discharge, aquaculture, etc.) adding more organic matter in coastal areas which consumes oxygen while being degraded *(Silva & Vargas, 2014)*. Within fjords, bathymetry is complex and numerous sills are trapping deep waters which, if they are warm (or hypoxic), can be cooled (or reoxygenated) only if new water replaces the one trapped by the sill or by mixing with upper layers. Thus, hypoxic conditions in Patagonian fjords might be enhanced by MHWs as thermal stratification would be increased by the water warming and as oxygen dissolution decreases when there is an SST rise *(Breitburg et al., 2018)*. Such conditions have already been observed in Norwegian deep-fjords where hypoxic conditions were exacerbated by deep waters warming, affecting benthic communities *(Aksnes et al., 2019)*.

6 CONCLUSION

This study presents, to the best of our knowledge, the first assessment of the marine heatwaves (MHWs) that have occurred along Central and South Chile (29°S-55°S), from 1982 to 2020. We found that, although MHWs were already present in the 1980s, their intensity and their duration has increased, particularly over the period 2012-2020, with record-breaking events. The Northern Patagonia (38°S-46°S) was the most hit region by these increasing MHWs trends, particularly over the last decade. For instance, in Northern Patagonia, 45% of all the MHWs that have occurred between 1982 and 2020 peaked after 2011 and 40% of the events that had an intensity superior to 1°C also occurred after 2011. In addition, we found that Northern Patagonia is the only Chilean coastal area where there is a long-term positive trend of MHWs frequency, probably related to the SST long-term warming trends, which also affect only the Northern Patagonia.

During the years 1997-1998 and in 2016, very strong El Niño conditions were reported, and were associated with positive phases of SAM. During these two periods, numerous MHWs occurred, some of them being among the longest and more intense ones.

Over the period 1982-2020, the year 2016 was the one during which Central Chile (29°S-38°S) experienced 110 days under MHWs conditions, Northern Patagonia 238 days and 188 days for Southern Patagonia (46°S-55°S). It was during that year that the longest MHW was recorded. Indeed, MHWs conditions persisted from May to October in Northern Patagonia and from June to October in Southern Patagonia. That event was caused by advection of warm-water anomalies from the extratropical Pacific and maintained by ideal atmospheric conditions, meaning a high-pressure system associated with lower winds and reduced heat transfer. Only a few days after the disappearance of this MHW, a new one peaked by the end of the year, being the strongest event recorded along Northern Patagonia and one of the most intense that have occurred along Southern Patagonia. That second MHW was triggered by warm-water anomalies coming from the tropical ocean, inducing shorter but more intense MHWs.

In this study we analysed the surface development of the MHWs. However, further works should be dedicated to the subsurface development of the MHWs which is also primordial as it will define the depth at which species will be affected by the warming. Additionally, further studies should assess how the inner seas of Patagonia are affected by MHWs. Indeed, MHWs consequences added to the already existing hypoxia and to the global warming might severely damage fjords ecosystems and aquaculture production.

7 REFERENCES

Aceituno, P., Boisier, J. P., Garreaud, R., Rondanelli, R., & Rutllant, J. A. (2021). Chapter 2: Climate and Weather in Chile. In B. Fernández & J. Gironás (Eds.), *Water Resources of Chile* (Vol. 8, pp. 129–151). Springer International Publishing. https://doi.org/10.1007/978-3-030-56901-3

Aguirre, C., García-Loyola, S., Testa, G., Silva, D., & Farías, L. (2018). Insight into anthropogenic forcing on coastal upwelling off south-central Chile. *Elementa: Science of the Anthropocene*, *6*, 59. https://doi.org/10.1525/elementa.314

Aksnes, D. L., Aure, J., Johansen, P.-O., Johnsen, G. H., & Vea Salvanes, A. G. (2019). Multi-decadal warming of Atlantic water and associated decline of dissolved oxygen in a deep fjord. *Estuarine, Coastal and Shelf Science*, *228*, 106392. https://doi.org/10.1016/j.ecss.2019.106392

Alvera-Azcárate, A., Barth, A., Rixen, M., & Beckers, J. M. (2005). Reconstruction of incomplete oceanographic data sets using empirical orthogonal functions: Application to the Adriatic Sea surface temperature. *Ocean Modelling*, *9*(4), 325–346. https://doi.org/10.1016/j.ocemod.2004.08.001

Ancapichún, S., & Garcés-Vargas, J. (2015). Variability of the Southeast Pacific Subtropical Anticyclone and its impact on sea surface temperature off north-central Chile. *Ciencias Marinas*, *41*(1), 1–20. https://doi.org/10.7773/cm.v41i1.2338

Arafeh-Dalmau, N., Montaño-Moctezuma, G., Martínez, J. A., Beas-Luna, R., Schoeman, D. S., & Torres-Moye, G. (2019). Extreme Marine Heatwaves Alter Kelp Forest Community Near Its Equatorward Distribution Limit. *Frontiers in Marine Science*, *6*, 499. https://doi.org/10.3389/fmars.2019.00499

Arias-Ortiz, A., Serrano, O., Masqué, P., Lavery, P. S., Mueller, U., Kendrick, G. A., Rozaimi, M., Esteban, A., Fourqurean, J. W., Marbà, N., Mateo, M. A., Murray, K., Rule, M. J., & Duarte, C. M. (2018). A marine heatwave drives massive losses from the world's largest seagrass carbon stocks. *Nature Climate Change*, *8*(4), 338–344. https://doi.org/10.1038/s41558-018-0096-y

Armijo, J., Oerder, V., Auger, P.-A., Bravo, A., & Molina, E. (2020). The 2016 red tide crisis in southern Chile: Possible influence of the mass oceanic dumping of dead salmons. *Marine Pollution Bulletin*, *150*. https://doi.org/10.1016/j.marpolbul.2019.110603

Barange, M., Bahri, T., Beveridge, M. C. M., Cochrane, K. L., Funge-Smith, S., & Poulain, F. (2018). *Impacts of climate change on fisheries and aquaculture: Synthesis of current knowledge, adaptation and mitigation options* (FAO, Vol. 627). http://www.fao.org/3/i9705en/i9705en.pdf

Barbeaux, S., Aydin, K., Fissel, B., Holsman, K., Palsson, W., Shotwell, K., Yang, Q., & Zador, S. (2018). Chapter 2: Assessment of the Pacific cod stock in the Gulf of Alaska. In *North Pacific Fishery Management Council* (Gulf of Alaska Stock Assessment and Fishery Evaluation Repport, p. 160).

Barbeaux, S. J., Holsman, K., & Zador, S. (2020). Marine Heatwave Stress Test of Ecosystem-Based Fisheries Management in the Gulf of Alaska Pacific Cod Fishery. *Frontiers in Marine Science*, *7*, 703. https://doi.org/10.3389/fmars.2020.00703

Beckers, J. M., & Rixen, M. (2003). EOF Calculations and Data Filling from Incomplete Oceanographic Datasets. *Journal of Atmospheric and Oceanic Technology*, *20*(12), 1839–1856.

Benthuysen, J. A., Oliver, E. C. J., Feng, M., & Marshall, A. G. (2018). Extreme Marine Warming Across Tropical Australia During Austral Summer 2015–2016. *Journal of Geophysical Research: Oceans*, *123*(2), 1301–1326. https://doi.org/10.1002/2017JC013326

Benthuysen, J., Feng, M., & Zhong, L. (2014). Spatial patterns of warming off Western Australia during the 2011 Ningaloo Niño: Quantifying impacts of remote and local forcing. *Continental Shelf Research*, *91*, 232–246. https://doi.org/10.1016/j.csr.2014.09.014

Black, E., Blackburn, M., Harrison, G., Hoskins, B., & Methven, J. (2004). Factors contributing to the summer 2003 European heatwave. *Weather*, *59*(8), 217–223. https://doi.org/10.1256/wea.74.04

Boisier, J. P., Rondanelli, R., Garreaud, R., & Muñoz, F. (2016). Anthropogenic and natural contributions to the Southeast Pacific precipitation decline and recent megadrought in central Chile. *Geophysical Research Letters*, *43*(1), 413–421. https://doi.org/10.1002/2015GL067265

Bond, N. A., Cronin, M. F., Freeland, H., & Mantua, N. (2015). Causes and impacts of the 2014 warm anomaly in the NE Pacific. *Geophysical Research Letters*, *42*(9), 3414–3420. https://doi.org/10.1002/2015GL063306

Brauko, K. M., Cabral, A., Costa, N. V., Hayden, J., Dias, C. E. P., Leite, E. S., Westphal, R. D., Mueller, C. M., Hall-Spencer, J. M., Rodrigues, R. R., Rörig, L. R., Pagliosa, P. R., Fonseca, A. L., Alarcon, O. E., & Horta, P. A. (2020). Marine Heatwaves, Sewage and Eutrophication Combine to Trigger Deoxygenation and Biodiversity Loss: A SW Atlantic Case Study. *Frontiers in Marine Science*, *7*. https://doi.org/10.3389/fmars.2020.590258

Breitburg, D., Levin, L. A., Oschlies, A., Grégoire, M., Chavez, F. P., Conley, D. J., Garçon, V., Gilbert, D., Gutiérrez, D., Isensee, K., Jacinto, G. S., Limburg, K. E., Montes, I., Naqvi, S. W. A., Pitcher, G. C., Rabalais, N. N., Roman, M. R., Rose, K. A., Seibel, B. A., … Zhang, J. (2018). Declining oxygen in the global ocean and coastal waters. *Science*, *359*(6371). https://doi.org/10.1126/science.aam7240

Caputi, N., Kangas, M., Denham, A., Feng, M., Pearce, A., Hetzel, Y., & Chandrapavan, A. (2016). Management adaptation of invertebrate fisheries to an extreme marine heat wave event at a global warming hot spot. *Ecology and Evolution*, *6*(11), 3583–3593. https://doi.org/10.1002/ece3.2137

Carvalho, K. S., Smith, T. E., & Wang, S. (2021). Bering Sea marine heatwaves: Patterns, trends and connections with the Arctic. *Journal of Hydrology*, *600*. https://doi.org/10.1016/j.jhydrol.2021.126462

Cavole, L., Demko, A., Diner, R., Giddings, A., Koester, I., Pagniello, C., Paulsen, M.-L., Ramirez-Valdez, A., Schwenck, S., Yen, N., Zill, M., & Franks, P. (2016). Biological Impacts of the 2013–2015 Warm-Water Anomaly in the Northeast Pacific: Winners, Losers, and the Future. *Oceanography*, *29*(2), 273–285. https://doi.org/10.5670/oceanog.2016.32

Chatterjee, S., Nuncio, M., & Satheesan, K. (2017). ENSO related SST anomalies and relation with surface heat fluxes over south Pacific and Atlantic. *Climate Dynamics*, *49*(1–2), 391–401. https://doi.org/10.1007/s00382-016-3349-3

Chavez, F. P., Bertrand, A., Guevara-Carrasco, R., Soler, P., & Csirke, J. (2008). The northern Humboldt Current System: Brief history, present status and a view towards the future. *Progress in Oceanography*, *79*(2–4), 95–105.

https://doi.org/10.1016/j.pocean.2008.10.012

Chen, N., Thual, S., & Hu, S. (2019). El Niño and the Southern Oscillation: Observation. In *Reference Module in Earth Systems and Environmental Sciences* (Elsevier). Elsevier. https://doi.org/10.1016/B978-0-12-409548-9.11766-X

Chen, N., Thual, S., & Stuecker, M. F. (2019). El Niño and the Southern Oscillation: Theory. In *Reference Module in Earth Systems and Environmental Sciences* (Elsevier). Elsevier. https://doi.org/10.1016/B978-0-12-409548-9.11765-8

Chen, Z., Shi, J., Liu, Q., Chen, H., & Li, C. (2021). A Persistent and Intense Marine Heatwave in the Northeast Pacific During 2019–2020. *Geophysical Research Letters*, *48*(13). https://doi.org/10.1029/2021GL093239

Cheung, W. W. L., & Frölicher, T. L. (2020). Marine heatwaves exacerbate climate change impacts for fisheries in the northeast Pacific. *Scientific Reports*, *10*(1), 6678. https://doi.org/10.1038/s41598-020-63650-z

Coleman, M. A., Minne, A. J. P., Vranken, S., & Wernberg, T. (2020). Genetic tropicalisation following a marine heatwave. *Scientific Reports*, *10*, 12726. https://doi.org/10.1038/s41598-020-69665-w

Couch, C. S., Burns, J. H. R., Liu, G., Steward, K., Gutlay, T. N., Kenyon, J., Eakin, C. M., & Kosaki, R. K. (2017). Mass coral bleaching due to unprecedented marine heatwave in Papahānaumokuākea Marine National Monument (Northwestern Hawaiian Islands). *PLOS ONE*, *12*(9). https://doi.org/10.1371/journal.pone.0185121

Dalton, S. J., Carroll, A. G., Sampayo, E., Roff, G., Harrison, P. L., Entwistle, K., Huang, Z., Salih, A., & Diamond, S. L. (2020). Successive marine heatwaves cause disproportionate coral bleaching during a fast phase transition from El Niño to La Niña. *Science of The Total Environment*, *715*. https://doi.org/10.1016/j.scitotenv.2020.136951

Darmaraki, S., Somot, S., Sevault, F., & Nabat, P. (2019). Past Variability of Mediterranean Sea Marine Heatwaves. *Geophysical Research Letters*, *46*(16), 9813–9823. https://doi.org/10.1029/2019GL082933

Deluqui-Gurgel, C. F. D., Camacho, O., Minne, A. J. P., Wernberg, T., & Coleman, M. A. (2020). Marine Heatwave Drives Cryptic Loss of Genetic Diversity in Underwater Forests. *Current Biology*, *30*(7), 1199–1206. https://doi.org/10.1016/j.cub.2020.01.051

Deutsch, C., Ferrel, A., Seibel, B., Portner, H.-O., & Huey, R. B. (2015). Climate change tightens a metabolic constraint on marine habitats. *Science*, *348*(6239), 1132–1135. https://doi.org/10.1126/science.aaa1605

Di Lorenzo, E., & Mantua, N. (2016). Multi-year persistence of the 2014/15 North Pacific marine heatwave. *Nature Climate Change*, *6*(11), 1042–1047. https://doi.org/10.1038/nclimate3082

Díaz, P. A., Álvarez, G., Varela, D., Pérez-Santos, I., Díaz, M., Molinet, C., Seguel, M., Aguilera-Belmonte, A., Guzmán, L., Uribe, E., Rengel, J., Hernández, C., Segura, C., & Figueroa, R. I. (2019). Impacts of harmful algal blooms on the aquaculture industry: Chile as a case study. *Perspectives in Phycology*, *6*(1–2), 39–50. https://doi.org/10.1127/pip/2019/0081

Ding, Q., Steig, E. J., Battisti, D. S., & Wallace, J. M. (2012). Influence of the Tropics on the Southern Annular Mode. *Journal of Climate*, *25*(18), 6330–6348. https://doi.org/10.1175/JCLI-D-11-00523.1

Eckstein, D., Hutfils, M.-L., & Winges, M. (2018). *Global Climate Risk Index 2019* (D.

Baum, J. Chapman-Rose, R. Hannes, & G. Kier, Eds.; Germanwatch).

Elliott, J. M., & Elliott, J. A. (2010). Temperature requirements of Atlantic salmon Salmo salar, brown trout Salmo trutta and Arctic charr Salvelinus alpinus: Predicting the effects of climate change. *Journal of Fish Biology*, *77*(8), 1793–1817. https://doi.org/10.1111/j.1095-8649.2010.02762.x

Estay, S. A., & Lima, M. (2010). Combined effect of ENSO and SAM on the population dynamics of the invasive yellowjacket wasp in central Chile. *Population Ecology*, *52*(2), 289–294. https://doi.org/10.1007/s10144-009-0179-8

FAO. (2019). Fishery and Aquaculture Statistics. Global aquaculture production 1950-2017 (FishstatJ). *In: FAO Fisheries and Aquaculture Department [Online]*.

Feng, M., McPhaden, M., Xie, S.-P., & Hafner, J. (2013). La Niña forces unprecedented Leeuwin Current warming in 2011. *Scientific Repport*, *3*, 1277. https://doi.org/10.1016/S0960-9822(97)70976-X

Filbee-Dexter, K., Wernberg, T., Grace, S. P., Thormar, J., Fredriksen, S., Narvaez, C. N., Feehan, C. J., & Norderhaug, K. M. (2020). Marine heatwaves and the collapse of marginal North Atlantic kelp forests. *Scientific Reports*, *10*(1), 13388. https://doi.org/10.1038/s41598-020-70273-x

Flores-Aqueveque, V., Rojas, M., Aguirre, C., Arias, P. A., & González, C. (2020). South Pacific Subtropical High from the late Holocene to the end of the 21st century: Insights from climate proxies and general circulation models. *Climate of the Past*, *16*(1), 79–99. https://doi.org/10.5194/cp-16-79-2020

Fogt, R. L., & Marshall, G. J. (2020). The Southern Annular Mode: Variability, trends, and climate impacts across the Southern Hemisphere. *WIREs Climate Change*, *11*(4). https://doi.org/10.1002/wcc.652

Frölicher, T. L., Fischer, E. M., & Gruber, N. (2018). Marine heatwaves under global warming. *Nature*, *560*(7718), 360–364. https://doi.org/10.1038/s41586-018-0383-9

Garrabou, J., Coma, R., Bensoussan, N., Bally, M., Chevaldonné, P., Cigliano, M., Diaz, D., Harmelin, J. G., Gambi, M. C., Kersting, D. K., Ledoux, J. B., Lejeusne, C., Linares, C., Marschal, C., Pérez, T., Ribes, M., Romano, J. C., Serrano, E., Teixido, N., … Cerrano, C. (2007). Mass mortality in Northwestern Mediterranean rocky benthic communities: Effects of the 2003 heat wave. *Global Change Biology*, *15*(5), 1090–1103. https://doi.org/10.1111/j.1365-2486.2008.01823.x

Garreaud, R. (2018a). Record-breaking climate anomalies lead to severe drought and environmental disruption in western Patagonia in 2016. *Climate Research*, *74*(3), 217–229. https://doi.org/10.3354/cr01505

Garreaud, R. (2018b). A plausible atmospheric trigger for the 2017 coastal El Niño. *International Journal of Climatology*, *38*, 1296–1302. https://doi.org/10.1002/joc.5426

Garreaud, R., Boisier, J. P., Rondanelli, R., Montecinos, A., Sepúlveda, H. H., & Veloso-Aguila, D. (2020). The Central Chile Mega Drought (2010–2018): A climate dynamics perspective. *International Journal of Climatology*, *40*(1), 421–439. https://doi.org/10.1002/joc.6219

Garreaud, R., Lopez, P., Minvielle, M., & Rojas, M. (2013). Large-Scale Control on the Patagonian Climate. *Journal of Climate*, *26*(1), 215–230. https://doi.org/10.1175/JCLI-D-12-00001.1

Garreaud, R., Vuille, M., Compagnucci, R., & Marengo, J. (2009). Present-day South American climate. *Palaeogeography, Palaeoclimatology, Palaeoecology*, *281*(3–4),

180–195. https://doi.org/10.1016/j.palaeo.2007.10.032

Gillett, N. P., & Thompson, D. (2003). Simulation of Recent Southern Hemisphere Climate Change. *Science*, *302*(5643), 273–275. https://doi.org/10.1126/science.1087440

Gong, D., & Wang, S. (1999). Definition of Antarctic Oscillation index. *Geophysical Research Letters*, *26*(4), 459–462. https://doi.org/10.1029/1999GL900003

Gong, T., Feldstein, S. B., & Luo, D. (2010). The Impact of ENSO on Wave Breaking and Southern Annular Mode Events. *Journal of the Atmospheric Sciences*, *67*(9), 2854–2870. https://doi.org/10.1175/2010JAS3311.1

Green, T. J., Montagnani, C., Benkendorff, K., Robinson, N., & Speck, P. (2014). Ontogeny and water temperature influences the antiviral response of the Pacific oyster, Crassostrea gigas. *Fish & Shellfish Immunology*, *36*(1), 151–157. https://doi.org/10.1016/j.fsi.2013.10.026

Greene, C. A., Thirumalai, K., Kearney, K. A., Delgado, J. M., Schwanghart, W., Wolfenbarger, N. S., Thyng, K. M., Gwyther, D. E., Gardner, A. S., & Blankenship, D. D. (2019). The Climate Data Toolbox for MATLAB. *Geochemistry, Geophysics, Geosystems*, *20*(7), 3774–3781. https://doi.org/10.1029/2019GC008392

Guan, Y., Zhu, J., Huang, B., Hu, Z.-Z., & Kinter III, J. L. (2014). South Pacific Ocean Dipole: A Predictable Mode on Multiseasonal Time Scales. *Journal of Climate*, *27*(4), 1648–1658. https://doi.org/10.1175/JCLI-D-13-00293.1

Gutiérrez, M. H., Narváez, D., Daneri, G., Montero, P., Pérez-Santos, I., & Pantoja, S. (2018). Linking Seasonal Reduction of Microbial Diversity to Increase in Winter Temperature of Waters of a Chilean Patagonia Fjord. *Frontiers in Marine Science*, *5*, 277. https://doi.org/10.3389/fmars.2018.00277

Hevrøy, E. M., Waagbø, R., Torstensen, B. E., Takle, H., Stubhaug, I., Jørgensen, S. M., Torgersen, T., Tvenning, L., Susort, S., Breck, O., & Hansen, T. (2012). Ghrelin is involved in voluntary anorexia in Atlantic salmon raised at elevated sea temperatures. *General and Comparative Endocrinology*, *175*(1), 118–134. https://doi.org/10.1016/j.ygcen.2011.10.007

Hobday, A. J., Alexander, L. V., Perkins, S. E., Smale, D. A., Straub, S. C., Oliver, E. C. J., Benthuysen, J. A., Burrows, M. T., Donat, M. G., Feng, M., Holbrook, N. J., Moore, P. J., Scannell, H. A., Sen Gupta, A., & Wernberg, T. (2016). A hierarchical approach to defining marine heatwaves. *Progress in Oceanography*, *141*, 227–238. https://doi.org/10.1016/j.pocean.2015.12.014

Hobday, A., Oliver, E., Sen Gupta, A., Benthuysen, J., Burrows, M., Donat, M., Holbrook, N., Moore, P., Thomsen, M., Wernberg, T., & Smale, D. (2018). Categorizing and Naming Marine Heatwaves. *Oceanography*, *31*(2), 162–173. https://doi.org/10.5670/oceanog.2018.205

Holbrook, N. J., Scannell, H. A., Sen Gupta, A., Benthuysen, J. A., Feng, M., Oliver, E. C. J., Alexander, L. V., Burrows, M. T., Donat, M. G., Hobday, A. J., Moore, P. J., Perkins-Kirkpatrick, S. E., Smale, D. A., Straub, S. C., & Wernberg, T. (2019). A global assessment of marine heatwaves and their drivers. *Nature Communications*, *10*(2624). https://doi.org/10.1038/s41467-019-10206-z

Holbrook, N. J., Sen Gupta, A., Oliver, E. C. J., Hobday, A. J., Benthuysen, J. A., Scannell, H. A., Smale, D. A., & Wernberg, T. (2020). Keeping pace with marine heatwaves. *Nature Reviews Earth & Environment*, *1*(9), 482–493. https://doi.org/10.1038/s43017-020-0068-4

Hu, L. (2021). A Global Assessment of Coastal Marine Heatwaves and Their Relation With Coastal Urban Thermal Changes. *Geophysical Research Letters*, *48*(9). https://doi.org/10.1029/2021GL093260

Hu, S., Zhang, L., & Qian, S. (2020). Marine Heatwaves in the Arctic Region: Variation in Different Ice Covers. *Geophysical Research Letters*, *47*(16). https://doi.org/10.1029/2020GL089329

IPCC. (2021). IPCC, 2021: Summary for Policymakers. *Climate Change 2021: The Physical Science Basis.*, *1*.

Iriarte, J. L. (2018). Natural and Human Influences on Marine Processes in Patagonian Subantarctic Coastal Waters. *Frontiers in Marine Science*, *5*, 360. https://doi.org/10.3389/fmars.2018.00360

Jackson, J. M., Johnson, G. C., Dosser, H. V., & Ross, T. (2018). Warming From Recent Marine Heatwave Lingers in Deep British Columbia Fjord. *Geophysical Research Letters*, *45*(18), 9757–9764. https://doi.org/10.1029/2018GL078971

Jacox, M. G. (2019). Marine heatwaves in a changing climate. *Nature*, *571*(7766), 485–487. https://doi.org/10.1038/d41586-019-02196-1

Jacox, M. G., Alexander, M. A., Bograd, S. J., & Scott, J. D. (2020). Thermal displacement by marine heatwaves. *Nature*, *584*(7819), 82–86. https://doi.org/10.1038/s41586-020-2534-z

Jacox, M. G., Hazen, E. L., Zaba, K. D., Rudnick, D. L., Edwards, C. A., Moore, A. M., & Bograd, S. J. (2016). Impacts of the 2015–2016 El Niño on the California Current System: Early assessment and comparison to past events. *Geophysical Research Letters*, *43*(13), 7072–7080. https://doi.org/10.1002/2016GL069716

Laufkötter, C., Zscheischler, J., & Frölicher, T. L. (2020). High-impact marine heatwaves attributable to human-induced global warming. *Science*, *369*(6511), 1621–1625. https://doi.org/10.1126/science.aba0690

Le Nohaïc, M., Ross, C. L., Cornwall, C. E., Comeau, S., Lowe, R., McCulloch, M. T., & Schoepf, V. (2017). Marine heatwave causes unprecedented regional mass bleaching of thermally resistant corals in northwestern Australia. *Scientific Reports*, *7*. https://doi.org/10.1038/s41598-017-14794-y

Lee, D. Y., Petersen, M. R., & Lin, W. (2019). The Southern Annular Mode and Southern Ocean Surface Westerly Winds in E3SM. *Earth and Space Science*, *6*(12), 2624–2643. https://doi.org/10.1029/2019EA000663

León-Muñoz, J., Urbina, M. A., Garreaud, R., & Iriarte, J. L. (2018). Hydroclimatic conditions trigger record harmful algal bloom in western Patagonia (summer 2016). *Scientific Reports*, *8*(1), 1330. https://doi.org/10.1038/s41598-018-19461-4

Letelier, J., Pizarro, O., & Nuñez, S. (2009). Seasonal variability of coastal upwelling and the upwelling front off central Chile. *Journal of Geophysical Research*, *114*. https://doi.org/10.1029/2008JC005171

L'Heureux, M. L., & Thompson, D. W. J. (2006). Observed Relationships between the El Niño–Southern Oscillation and the Extratropical Zonal-Mean Circulation. *Journal of Climate*, *19*(2), 276–287. https://doi.org/10.1175/JCLI3617.1

Li, G., Li, C., Tan, Y., & Bai, T. (2012). Seasonal evolution of dominant modes in south pacific SST and relationship with ENSO. *Advances in Atmospheric Sciences*, *29*(6), 1238–1248. https://doi.org/10.1007/s00376-012-1191-z

Lima, F. P., & Wethey, D. S. (2012). Three decades of high-resolution coastal sea surface

temperatures reveal more than warming. *Nature Communications*, *3*(704). https://doi.org/10.1038/ncomms1713

Lonhart, S. I., Jeppesen, R., Beas-Luna, R., Crooks, J. A., & Lorda, J. (2019). Shifts in the distribution and abundance of coastal marine species along the eastern Pacific Ocean during marine heatwaves from 2013 to 2018. *Marine Biodiversity Records*, *12*. https://doi.org/10.1186/s41200-019-0171-8

Manta, G., Mello, S., Trinchin, R., Badagian, J., & Barreiro, M. (2018). The 2017 Record Marine Heatwave in the Southwestern Atlantic Shelf. *Geophysical Research Letters*, *45*(22), 12,449-12,456. https://doi.org/10.1029/2018GL081070

Mantua, N., Hare, S., Zhang, Y., Wallace, J., & Francis, R. (1997). A Pacific interdecadal climate oscillation with impacts on salmon production. *Bulletin of the American Meteorological Society*, *78*, 1069–1079.

Mantua, N. J., & Hare, S. R. (2002). The Pacific Decadal Oscillation. *Journal of Oceanography*, *58*, 35–44. https://doi.org/10.1023/A:1015820616384

Marshall, G. J. (2003). Trends in the Southern Annular Mode from Observations and Reanalyses. *Journal of Climate*, *16*(24), 4134–4143.

Mawren, D., Hermes, J., & Reason, C. J. C. (2021). Marine heatwaves in the Mozambique Channel. *Climate Dynamics*. https://doi.org/10.1007/s00382-021-05909-3

McCabe, R. M., Hickey, B. M., Kudela, R. M., Lefebvre, K. A., Adams, N. G., Bill, B. D., Gulland, F. M. D., Thomson, R. E., Cochlan, W. P., & Trainer, V. L. (2016). An unprecedented coastwide toxic algal bloom linked to anomalous ocean conditions. *Geophysical Research Letters*, *43*(19), 10366–10376. https://doi.org/10.1002/2016GL070023

McPhee, J., MacDoell, S., & Casassa, G. (2021). Chapter 6: Snow Cover and Glaciers. In B. Fernández & J. Gironás (Eds.), *Water Resources of Chile* (Vol. 8). Springer International Publishing. https://doi.org/10.1007/978-3-030-56901-3

McPherson, M. L., Finger, D. J. I., Houskeeper, H. F., Bell, T. W., Carr, M. H., Rogers-Bennett, L., & Kudela, R. M. (2021). Large-scale shift in the structure of a kelp forest ecosystem co-occurs with an epizootic and marine heatwave. *Communications Biology*, *4*(1), 298. https://doi.org/10.1038/s42003-021-01827-6

Mignot, A., Von Schuckmann, K., Gasparin, F., van Gennip, S., Landschützer, P., Perruche, C., Lamouroux, J., & Amm, T. (Preprint). *Decrease in air-sea CO2 fluxes caused by persistent marine heatwaves* [Preprint]. https://doi.org/10.31223/X5JG7V

Mills, K., Pershing, A., Brown, C., Chen, Y., Chiang, F.-S., Holland, D., Lehuta, S., Nye, J., Sun, J., Thomas, A., & Wahle, R. (2013). Fisheries Management in a Changing Climate: Lessons From the 2012 Ocean Heat Wave in the Northwest Atlantic. *Oceanography*, *26*(2). https://doi.org/10.5670/oceanog.2013.27

Miyama, T., Minobe, S., & Goto, H. (2021). Marine Heatwave of Sea Surface Temperature of the Oyashio Region in Summer in 2010–2016. *Frontiers in Marine Science*, *7*, 1150. https://doi.org/10.3389/fmars.2020.576240

Montecinos, A., & Aceituno, P. (2003). Seasonality of the ENSO-Related Rainfall Variability in Central Chile and Associated Circulation Anomalies. *Journal of Climate*, *16*(2), 281–296. https://doi.org/10.1175/1520-0442(2003)016<0281:SOTERR>2.0.CO;2

Montecinos, A., & Gomez, F. (2010). ENSO modulation of the upwelling season off southern-central Chile. *Geophysical Research Letters*, *37*(2). https://doi.org/10.1029/2009GL041739

Morrison, M., Lowe, M. L., Grant, C. M., Smith, P. J., Carbines, G. D., Reed, J., Bury, S., & Brown, J. (2014). Seagrass meadows as biodiversity and productivity hotspots. *New Zealand Aquaitic Biodiversity and Biosecurity Series*. http://fs.fish.govt.nz/Doc/23703/AEBR_137_2701_ZBD2004-08%20Objective%201-4;%20Milestones%208,9,10,17,18,23,24,%2025,28,29%20and%2030.pdf.ashx

Myers, T. A., Mechoso, C. R., Cesana, G. V., DeFlorio, M. J., & Waliser, D. E. (2018). Cloud Feedback Key to Marine Heatwave off Baja California. *Geophysical Research Letters*, *45*(9), 4345–4352. https://doi.org/10.1029/2018GL078242

Newman, M., Alexander, M. A., Ault, T. R., Cobb, K. M., Deser, C., Di Lorenzo, E., Mantua, N. J., Miller, A. J., Minobe, S., Nakamura, H., Schneider, N., Vimont, D. J., Phillips, A. S., Scott, J. D., & Smith, C. A. (2016). The Pacific Decadal Oscillation, Revisited. *Journal of Climate*, *29*(12), 4399–4427. https://doi.org/10.1175/JCLI-D-15-0508.1

NOAA Climate, (National Oceanic and Atmospheric Administration Climate). (2014). *The Walker Circulation: ENSO's atmospheric buddy*. https://www.climate.gov/news-features/blogs/enso/walker-circulation-ensos-atmospheric-buddy

NOAA Climate, (National Oceanic and Atmospheric Administration Climate). (2015). *Record-setting bloom of toxic algae in North Pacific*. https://www.climate.gov/news-features/event-tracker/record-setting-bloom-toxic-algae-north-pacific

Olita, A., Sorgente, R., Natale, S., Gaberšek, S., Ribotti, A., Bonanno, A., & Patti, B. (2007). Effects of the 2003 European heatwave on the Central Mediterranean Sea: Surface fluxes and the dynamical response. *Ocean Science*, *3*(2), 273–289. https://doi.org/10.5194/os-3-273-2007

Oliver, E. C. J., Benthuysen, J. A., Bindoff, N. L., Hobday, A. J., Holbrook, N. J., Mundy, C. N., & Perkins-Kirkpatrick, S. E. (2017). The unprecedented 2015/16 Tasman Sea marine heatwave. *Nature Communications*, *8*(16101). https://doi.org/10.1038/ncomms16101

Oliver, E. C. J., Benthuysen, J. A., Darmaraki, S., Donat, M. G., Hobday, A. J., Holbrook, N. J., Schlegel, R. W., & Sen Gupta, A. (2021). Marine Heatwaves. *Annual Review of Marine Science*, *13*(1), 313–342. https://doi.org/10.1146/annurev-marine-032720-095144

Oliver, E. C. J., Burrows, M. T., Donat, M. G., Sen Gupta, A., Alexander, L. V., Perkins-Kirkpatrick, S. E., Benthuysen, J. A., Hobday, A. J., Holbrook, N. J., Moore, P. J., Thomsen, M. S., Wernberg, T., & Smale, D. A. (2019). Projected Marine Heatwaves in the 21st Century and the Potential for Ecological Impact. *Frontiers in Marine Science*, *6*, 734. https://doi.org/10.3389/fmars.2019.00734

Oliver, E. C. J., Donat, M. G., Burrows, M. T., Moore, P. J., Smale, D. A., Alexander, L. V., Benthuysen, J. A., Feng, M., Sen Gupta, A., Hobday, A. J., Holbrook, N. J., Perkins-Kirkpatrick, S. E., Scannell, H. A., Straub, S. C., & Wernberg, T. (2018). Longer and more frequent marine heatwaves over the past century. *Nature Communications*, *9*(1324). https://doi.org/10.1038/s41467-018-03732-9

Omneya, I., Bayoumy, M., & Hazem, N. (2021). Spatial Variability and Trends of Marine Heat Waves in the Eastern Mediterranean Sea over 39 Years. *Journal of Marine Science and Engineering*, *9*(6), 643. https://doi.org/10.3390/jmse9060643

Orsi, A. H., Whitworth, T., & Nowlin, W. D. (1995). On the meridional extent and fronts of the Antarctic Circumpolar Current. *Deep Sea Research Part I: Oceanographic Research Papers*, *42*(5), 641–673. https://doi.org/10.1016/0967-0637(95)00021-W

Pantoja, S., Iriarte, J. L., & Daneri, G. (2011). Oceanography of the Chilean Patagonia.

Continental Shelf Research, *31*(3–4), 149–153. https://doi.org/10.1016/j.csr.2010.10.013

Pearce, A. F., & Feng, M. (2013). The rise and fall of the "marine heat wave" off Western Australia during the summer of 2010/2011. *Journal of Marine Systems*, *111–112*, 139–156. https://doi.org/10.1016/j.jmarsys.2012.10.009

Pearce, A., Lenanton, R., Jackson, G., & Gaughan, D. (2011). *The 'marine heat wave' off Western Australia during the summer of 2010/11* (No. 222; Fisheries Research Repport, p. 40). Department of Fisheries, Western Australia.

Pérez-Santos, I., Castro, L., Ross, L., Niklitschek, E., Mayorga, N., Cubillos, L., Gutierrez, M., Escalona, E., Castillo, M., Alegría, N., & Daneri, G. (2018). Turbulence and hypoxia contribute to dense biological scattering layers in a Patagonian fjord system. *Ocean Science*, *14*(5), 1185–1206. https://doi.org/10.5194/os-14-1185-2018

Perkins-Kirkpatrick, S. E., King, A. D., Cougnon, E. A., Holbrook, N. J., Grose, M. R., Oliver, E. C. J., Lewis, S. C., & Pourasghar, F. (2019). The Role of Natural Variability and Anthropogenic Climate Change in the 2017/18 Tasman Sea Marine Heatwave. *Bulletin of the American Meteorological Society*, *100*(1), 105–110. https://doi.org/10.1175/BAMS-D-18-0116.1

Pizarro, O., Hormazabal, S., Gonzalez, A., & Yañez, E. (1994). Variabilidad del viento, nivel del mar y temperatura en la costa norte de Chile. *Investigaciones marinas*, *22*, 85–101. https://doi.org/10.4067/S0717-71781994002200007

Porter, C., & Santana, A. (2014). Rápido Retroceso, en el Siglo 20, del ventisquero Marinelli en el campo de Hielo de la Cordillera Darwin. Rapid 20th Century Retreat of Ventisquero Marinelli in the Cordillera Darwin Icefield. *Anales Del Instituto De La Patagonia*, *37*, 17–26.

Rahn, D. A., & Garreaud, R. (2014). A synoptic climatology of the near-surface wind along the west coast of South America. *International Journal of Climatology*, *34*(3), 780–792. https://doi.org/10.1002/joc.3724

Reaka-Kudla, M. L. (1997). The global biodiversity of coral reefs: A comparison with rainforests. In *Biodiversity II: Understanding and Protecting Our Biological Resources* (pp. 83–108). M. L. Reaka-Kudla, D. E. Wilson, and E. O. Wilson (Washington, DC: Joseph Henry Press).

Reboita, M. S., Ambrizzi, T., & Rocha, R. P. da. (2009). Relationship between the southern annular mode and southern hemisphere atmospheric systems. *Revista Brasileira de Meteorologia*, *24*(1), 48–55. https://doi.org/10.1590/S0102-77862009000100005

Rind, D., Chandler, M., Lerner, J., Martinson, D. G., & Yuan, X. (2001). Climate response to basin-specific changes in latitudinal temperature gradients and implications for sea ice variability. *Journal of Geophysical Research: Atmospheres*, *106*(D17), 20161–20173. https://doi.org/10.1029/2000JD900643

Roberts, S. D., Van Ruth, P. D., Wilkinson, C., Bastianello, S. S., & Bansemer, M. S. (2019). Marine Heatwave, Harmful Algae Blooms and an Extensive Fish Kill Event During 2013 in South Australia. *Frontiers in Marine Science*, *6*, 610. https://doi.org/10.3389/fmars.2019.00610

Rodríguez-Morata, C., Díaz, H. F., Ballesteros-Canovas, J. A., Rohrer, M., & Stoffel, M. (2019). The anomalous 2017 coastal El Niño event in Peru. *Climate Dynamics*, *52*(9–10), 5605–5622. https://doi.org/10.1007/s00382-018-4466-y

Roemmich, D., Gilson, J., Sutton, P., & Zilberman, N. (2016). Multidecadal Change of the

South Pacific Gyre Circulation. *Journal of Physical Oceanography*, *46*(6), 1871–1883. https://doi.org/10.1175/JPO-D-15-0237.1

Rutllant, J., & Fuenzalida, H. (1991). Synoptic aspects of the central chile rainfall variability associated with the southern oscillation. *International Journal of Climatology*, *11*(1), 63–76. https://doi.org/10.1002/joc.3370110105

Rutterford, L. A., Simpson, S. D., Jennings, S., Johnson, M. P., Blanchard, J. L., Schön, P.-J., Sims, D. W., Tinker, J., & Genner, M. J. (2015). Future fish distributions constrained by depth in warming seas. *Nature Climate Change*, *5*(6), 569–573. https://doi.org/10.1038/nclimate2607

Salinger, M. J., Renwick, J., Behrens, E., Mullan, A. B., Diamond, H. J., Sirguey, P., Smith, R. O., Trought, M. C. T., Alexander, L., Cullen, N. J., Fitzharris, B. B., Hepburn, C. D., Parker, A. K., & Sutton, P. J. (2019). The unprecedented coupled ocean-atmosphere summer heatwave in the New Zealand region 2017/18: Drivers, mechanisms and impacts. *Environmental Research Letters*, *14*(4). https://doi.org/10.1088/1748-9326/ab012a

Santora, J. A., Mantua, N. J., Schroeder, I. D., Field, J. C., Hazen, E. L., Bograd, S. J., Sydeman, W. J., Wells, B. K., Calambokidis, J., Saez, L., Lawson, D., & Forney, K. A. (2020). Habitat compression and ecosystem shifts as potential links between marine heatwave and record whale entanglements. *Nature Communications*, *11*(1), 536. https://doi.org/10.1038/s41467-019-14215-w

Santoso, A., McPhaden, M., & Cai, W. (2017). The defining characteristics of ENSO extremes and the strong 2015/2016 El Niño. *Reviews of Geophysics*, *55*, 1079–1129. https://doi.org/10.1002/2017RG000560

Saurral, R. I., García-Serrano, J., Doblas-Reyes, F. J., Díaz, L. B., & Vera, C. S. (2020). Decadal predictability and prediction skill of sea surface temperatures in the South Pacific region. *Climate Dynamics*, *54*(9–10), 3945–3958. https://doi.org/10.1007/s00382-020-05208-3

Scannell, H. A., Pershing, A. J., Alexander, M. A., Thomas, A. C., & Mills, K. E. (2016). Frequency of marine heatwaves in the North Atlantic and North Pacific since 1950: FREQUENCY OF MARINE HEATWAVES SINCE 1950. *Geophysical Research Letters*, *43*(5), 2069–2076. https://doi.org/10.1002/2015GL067308

Schär, C., Vidale, P. L., Lüthi, D., Frei, C., Häberli, C., Liniger, M. A., & Appenzeller, C. (2004). The role of increasing temperature variability in European summer heatwaves. *Nature*, *427*(6972), 332–336. https://doi.org/10.1038/nature02300

Schmeisser, L., Bond, N. A., Siedlecki, S. A., & Ackerman, T. P. (2019). The Role of Clouds and Surface Heat Fluxes in the Maintenance of the 2013–2016 Northeast Pacific Marine Heatwave. *Journal of Geophysical Research: Atmospheres*, *124*(20), 10772–10783. https://doi.org/10.1029/2019JD030780

Schneider, W., Pérez-Santos, I., Ross, L., Bravo, L., Seguel, R., & Hernández, F. (2014). On the hydrography of Puyuhuapi Channel, Chilean Patagonia. *Progress in Oceanography*, *129*, 8–18. https://doi.org/10.1016/j.pocean.2014.03.007

Sen Gupta, A., Thomsen, M., Benthuysen, J. A., Hobday, A. J., Oliver, E., Alexander, L. V., Burrows, M. T., Donat, M. G., Feng, M., Holbrook, N. J., Perkins-Kirkpatrick, S., Moore, P. J., Rodrigues, R. R., Scannell, H. A., Taschetto, A. S., Ummenhofer, C. C., Wernberg, T., & Smale, D. A. (2020). Drivers and impacts of the most extreme marine heatwaves events. *Scientific Reports*, *10*(1), 19359. https://doi.org/10.1038/s41598-020-75445-3

Silva, N., & Vargas, C. A. (2014). Hypoxia in Chilean Patagonian Fjords. *Progress in Oceanography*, *129*, 62–74. https://doi.org/10.1016/j.pocean.2014.05.016

Smale, D. A., & Wernberg, T. (2013). Extreme climatic event drives range contraction of a habitat-forming species. *Proceedings of the Royal Society B: Biological Sciences*, *280*(1754). https://doi.org/10.1098/rspb.2012.2829

Smale, D. A., Wernberg, T., Oliver, E. C. J., Thomsen, M., Harvey, B. P., Straub, S. C., Burrows, M. T., Alexander, L. V., Benthuysen, J. A., Donat, M. G., Feng, M., Hobday, A. J., Holbrook, N. J., Perkins-Kirkpatrick, S. E., Scannell, H. A., Sen Gupta, A., Payne, B. L., & Moore, P. J. (2019). Marine heatwaves threaten global biodiversity and the provision of ecosystem services. *Nature Climate Change*, *9*(4), 306–312. https://doi.org/10.1038/s41558-019-0412-1

Sobarzo, M., Bravo, L., Donoso, D., Garcés-Vargas, J., & Schneider, W. (2007). Coastal upwelling and seasonal cycles that influence the water column over the continental shelf off central Chile. *Progress in Oceanography*, *75*(3), 363–382. https://doi.org/10.1016/j.pocean.2007.08.022

Soto, D., León-Muñoz, J., Dresdner, J., Luengo, C., Tapia, F. J., & Garreaud, R. (2019). Salmon farming vulnerability to climate change in southern Chile: Understanding the biophysical, socioeconomic and governance links. *Reviews in Aquaculture*, *11*(2), 354–374. https://doi.org/10.1111/raq.12336

Stramma, L., Peterson, R., & Tomczak, M. (1995). The South Pacific Current. *Journal of Physical Oceanography*, *25*(1), 77–91.

Strub, P. T., James, C., Montecino, V., Rutllant, J. A., & Blanco, J. L. (2019). Ocean circulation along the southern Chile transition region (38°–46°S): Mean, seasonal and interannual variability, with a focus on 2014–2016. *Progress in Oceanography*, *172*, 159–198. https://doi.org/10.1016/j.pocean.2019.01.004

Su, Z., Pilo, G. S., Corney, S., Holbrook, N. J., Mori, M., & Ziegler, P. (2021). Characterizing Marine Heatwaves in the Kerguelen Plateau Region. *Frontiers in Marine Science*, *7*, 1119. https://doi.org/10.3389/fmars.2020.531297

Tanaka, K. R., Van Houtan, K. S., Mailander, E., Dias, B. S., Galginaitis, C., O'Sullivan, J., Lowe, C. G., & Jorgensen, S. J. (2021). North Pacific warming shifts the juvenile range of a marine apex predator. *Scientific Reports*, *11*. https://doi.org/10.1038/s41598-021-82424-9

Thiel, M., Macaya, E., Acu√±a, E., Arntz, W., Bastias, H., Brokordt, K., Camus, P., Castilla, J., Castro, L., Cort√©s, M., Dumont, C., Escribano, R., Fernandez, M., Gajardo, J., Gaymer, C., Gomez, I., Gonz√°lez, A., Gonz√°lez, H., Haye, P., … Vega, A. (2007). The Humboldt Current System of Northern and Central Chile: Oceanographic Processes, Ecological Interactions And Socioeconomic Feedback. In R. Gibson, R. Atkinson, & J. Gordon (Eds.), *Oceanography and Marine Biology* (Vol. 20074975). CRC Press. https://doi.org/10.1201/9781420050943.ch6

Thompson, D. W. J., & Wallace, J. M. (2000). Annular Modes in the Extratropical Circulation. Part I: Month-to-Month Variability. *Journal of Climate*, *13*(5), 1000–1016.

Thomson, J. A., Burkholder, D. A., Heithaus, M. R., Fourqurean, J. W., Fraser, M. W., Statton, J., & Kendrick, G. A. (2015). Extreme temperatures, foundation species, and abrupt ecosystem change: An example from an iconic seagrass ecosystem. *Global Change Biology*, *21*(4), 1463–1474. https://doi.org/10.1111/gcb.12694

Varela, R., Rodríguez-Díaz, L., de Castro, M., & Gómez-Gesteira, M. (2021). Influence of

Eastern Upwelling systems on marine heatwaves occurrence. *Global and Planetary Change, 196*. https://doi.org/10.1016/j.gloplacha.2020.103379

Viale, M., & Garreaud, R. (2015). Orographic effects of the subtropical and extratropical Andes on upwind precipitating clouds. *Journal of Geophysical Research: Atmospheres, 120*(10), 4962–4974. https://doi.org/10.1002/2014JD023014

W. Schlegel, R., & J. Smit, A. (2018). heatwaveR: A central algorithm for the detection of heatwaves and cold-spells. *Journal of Open Source Software*, *3*(27), 821. https://doi.org/10.21105/joss.00821

Wade, N. M., Clark, T. D., Maynard, B. T., Atherton, S., Wilkinson, R. J., Smullen, R. P., & Taylor, R. S. (2019). Effects of an unprecedented summer heatwave on the growth performance, flesh colour and plasma biochemistry of marine cage-farmed Atlantic salmon (Salmo salar). *Journal of Thermal Biology*, *80*, 64–74. https://doi.org/10.1016/j.jtherbio.2018.12.021

Wang, G., & Cai, W. (2013). Climate-change impact on the 20th-century relationship between the Southern Annular Mode and global mean temperature. *Scientific Reports*, *3*(1), 2039. https://doi.org/10.1038/srep02039

Weitzman, B., Konar, B., Iken, K., Coletti, H., Monson, D., Suryan, R., Dean, T., Hondolero, D., & Lindeberg, M. (2021). Changes in Rocky Intertidal Community Structure During a Marine Heatwave in the Northern Gulf of Alaska. *Frontiers in Marine Science*, *8*, 115. https://doi.org/10.3389/fmars.2021.556820

Welch, C. (2015, January 24). Mass Death of Seabirds in Western U.S. Is 'Unprecedented'. *National Geographic*. https://www.nationalgeographic.com/science/article/150123-seabirds-mass-die-off-auklet-california-animals-environment

Wernberg, T., Smale, D. A., Tuya, F., Thomsen, M. S., Langlois, T. J., de Bettignies, T., Bennett, S., & Rousseaux, C. S. (2013). An extreme climatic event alters marine ecosystem structure in a global biodiversity hotspot. *Nature Climate Change*, *3*, 78–82. https://doi.org/10.1038/nclimate1627

Winckler-Grez, P. W., Aguirre, C., Farías, L., Contreras-López, M., & Masotti, Í. (2020). Evidence of climate-driven changes on atmospheric, hydrological, and oceanographic variables along the Chilean coastal zone. *Climatic Change*, *163*(2), 633–652. https://doi.org/10.1007/s10584-020-02805-3

Yáñez, E., Lagos, N. A., Norambuena, R., Silva, C., Letelier, J., Muck, K.-P., Martin, G. S., Benítez, S., R. Broitman, B., Contreras, H., Duarte, C., Gelcich, S., Labra, F. A., Lardies, M. A., Manríquez, P. H., Quijón, P. A., Ramajo, L., González, E., Molina, R., … Böhm, G. (2017). Impacts of Climate Change on Marine Fisheries and Aquaculture in Chile. In B. F. Phillips & M. Pérez-Ramírez (Eds.), *Climate Change Impacts on Fisheries and Aquaculture* (John Wiley&Sons Ltd, Vol. 1, pp. 239–332). John Wiley & Sons, Ltd. https://doi.org/10.1002/9781119154051.ch10

Zou, Y., & Xi, X. (2021). An ongoing cooling in the eastern Pacific linked to eastward migrations of the Southeast Pacific Subtropical Anticyclone. *Environmental Research Letters*, *16*(3). https://doi.org/10.1088/1748-9326/abd819